atmosphere

Review

Isoprene Emissions, Oxidation Chemistry and Environmental Impacts

M. Anwar H. Khan [1,*], Rayne Holland [1], Charlotte Mould [1], Asan Bacak [2,3], Carl J. Percival [4] and Dudley E. Shallcross [1,5,*]

1 School of Chemistry, University of Bristol, Cantock's Close, Bristol BS8 1TS, UK; rayne.holland@bristol.ac.uk (R.H.); cm17910@bristol.ac.uk (C.M.)
2 Ankara University Cancer Research Institute, Balkiraz Mahallesi, Mamak Caddesi No:1/8, 06620 Mamak, Ankara, Turkey; abacak@tarlafel.org
3 Turkish Accelerator & Radiation Laboratory, Ankara University, 06830 Golbasi, Ankara, Turkey
4 Jet Propulsion Laboratory, California Institute of Technology, 4800 Oak Grove Dr, Pasadena, CA 91109, USA; carl.j.percival@jpl.nasa.gov
5 Department of Chemistry, University of the Western Cape, Robert Sobukwe Road, Bellville 7305, South Africa
* Correspondence: anwar.khan@bristol.ac.uk (M.A.H.K.); d.e.shallcross@bristol.ac.uk (D.E.S.)

Abstract: Isoprene emissions can affect the oxidizing capacity of the atmosphere and are likely to increase with an increase in the world's biomass. The emission of isoprene is strongest in tropical forested regions, suggesting a major portion of tropospheric chemistry occurs in the tropics. As well as deforestation and reforestation having a direct impact on the world's climate through land cover, there is also an indirect environmental impact (e.g., global warming, air pollution) through the resulting change in isoprene emissions. Previously, incomplete understanding of isoprene oxidation chemistry caused a model-measurement breakdown for concentrations of HO_x radicals observed over certain low-NO_x regions, such as the pristine Amazon rainforest. Over the last decade, however, understanding of isoprene oxidation chemistry has been vastly improved. Numerous research studies have provided evidence for the involvement of 1,6-H and 1,5-H shift reactions in the isoprene oxidation mechanism, which increases the level of HO_x recycling that occurs. As well as helping to reduce the model-measurement breakdown observed, the updated isoprene oxidation mechanism affects the tropospheric burdens of other species, including carbon monoxide (CO), methane (CH_4), ozone (O_3), organic peroxides (ROOH), secondary organic aerosol (SOA), and organic nitrates ($RONO_2$). There are still gaps in the understanding of the impacts and oxidation chemistry of isoprene emissions, which this literature review identifies and discusses. In the future, there is still much scope for further research, including modeling future reforestation scenarios with isoprene emissions and their impacts on both global and regional scales.

Keywords: ozone; Amazon; climate change; deforestation; reforestation; oxidation mechanism; secondary organic aerosol

Academic Editor: Jianyin Xiong

Received: 17 January 2025
Revised: 18 February 2025
Accepted: 22 February 2025
Published: 24 February 2025

Citation: Khan, M.A.H.; Holland, R.; Mould, C.; Bacak, A.; Percival, C.J.; Shallcross, D.E. Isoprene Emissions, Oxidation Chemistry and Environmental Impacts. *Atmosphere* **2025**, *16*, 259. https://doi.org/10.3390/atmos16030259

1. Introduction

Terrestrial vegetation accounts for around 90% of the total atmospheric non-methane volatile organic compounds (VOCs) emission. Hence, this source dominates biogenic VOCs (BVOCs) emissions into the atmosphere [1]. Among BVOCs, isoprene (C_5H_8) has the largest emission flux, contributing approximately half of the total BVOCs (about 1000 TgC yr^{-1}) [2], and has been the focus of a significant amount of research in terms of the controlling factors of its emission, atmospheric oxidation chemistry, and subsequent environmental impacts.

A review of literature concerning isoprene emissions and its measurements, recent updates to isoprene oxidation chemistry and its environmental impacts, the impact of deforestation and reforestation on isoprene emissions, and its oxidation products are presented.

As isoprene is emitted mainly from terrestrial vegetation, its emissions are directly dependent on the land cover (e.g., tree, shrub, grass, crop) and on the plant species within those land covers [2,3]. Isoprene emissions from plants is directly linked to photosynthesis, as the formation of the C_5 compound is non-trivial, in fact requiring a significant amount of energy [4,5]. The production of isoprene occurs within plants during photosynthetic metabolism through the precursors dimethylallyl pyrophosphate (DMAPP) and isopentenyl pyrophosphate (IPP), with the former being the substrate for the isoprene synthase [6,7]. The isoprene synthase converts DMAPP to isoprene through cleavage of pyrophosphate, and emission of isoprene can subsequently occur, although it does so at significant cost to the plant in terms of carbon and adenosine triphosphate (ATP). Plants can release isoprene through other metabolic pathways when drought inhibits photosynthesis [8]. Algae, which are photosynthetic organisms, can produce isoprene in darkness [9–11]. Various bacteria can emit isoprene through enzymatic mechanisms [12–14]. Different root-associated fungi can emit isoprene, but its production mechanism is still undetermined [15]. The ocean is a source of isoprene to the atmosphere, but global isoprene emissions from the ocean are small (0.32–11.6 TgC yr^{-1}) [16–20] compared with the terrestrial sources. Isoprene is also emitted from vehicular exhaust [21–23] and human exhalation [24,25]. In addition to biogenic emissions, other emissions are found to contribute only approximately 15% (~100 TgC yr^{-1}) [26] of the total global isoprene emissions. In this review we will focus mainly on the biogenic emissions of isoprene and therefore discuss the biological controlling factors of its emission.

2. Biological Function of Isoprene Emission

In the literature review by Sharkey and Monson [27], isoprene biology is described as 'enigmatic'. Sixty years after its discovery, with many of its chemical reactions and biological synthetic pathways recognized, the scientific community still does not fully understand why plants evolved to emit isoprene in the first place, and indeed why they continue to do so. When categorizing isoprene-emitting species, a simple pattern is difficult to decipher. Many closely related species can differ in their emissions or capacity to emit altogether; European oaks, for example, produce insignificant levels of isoprene, whereas their closely related American counterparts are high emitters of the species [28]. One of the benefits of understanding the biological function of isoprene could be to help scientists better explain these interspecies differences. However, theories as to why plants emit isoprene have been emerging for years, with little definitive evidence for one argument over another [7]. The emission of isoprene is a metabolic cost for plants (starting from carbon dioxide (CO_2), 20 ATP and 14 Nicotinamide adenine dinucleotide phosphate (NADPH) per isoprene molecule [4]), but benefits may outweigh the cost, especially under high temperature [29] and oxidative stress [30].

A popular hypothesis as to the biological function of isoprene is thermotolerance. Specifically, protection against heat specks that arise when sunlight strikes a leaf and causes the surface to rapidly warm. A correlation between light exposure and isoprene emission was first reported in 1966, although this evolved into attributing more specifically the effect of the thermal excitation from light 30 years later [31,32]. This is consistent with findings that trees at the top of rainforest canopies emit the highest concentrations of isoprene, as they have to tolerate the highest radiation levels from the sun [33]. It was through this connection between daylight and isoprene emission that the direct relationship to photosynthesis was also established [5]. Isoprene protection against reactive oxygen species is another popular theory. Ozone (O_3) has been shown to damage the photosynthetic apparatus in plants, with an increase in external isoprene concentration counteracting the detrimental effect [34,35]. Similarly, it was found that the presence of isoprene in combination with nitric oxide (NO) could also be used against oxidative stress in the form of ozone or singlet oxygen [36]. Although, similarly to thermotolerance theories, the exact mechanisms of protection are not known, and counterarguments to these conclusions are also reported [37]. During the use of isoprene as an insect repellent, it has been shown to interfere with the chemoreceptors in some species of parasitic wasps, hindering their ability to locate the plant they sought to attack [38]. In a species of tobacco plant, isoprene has been shown to act as a deterrent to its damaging inhabitant, the tobacco caterpillar [39]. The relationship between animal and plant will not be discussed further, but it is worth mentioning its significance, as plants may have evolved isoprene emission for protection against a variety of stressors.

Through the dependence of isoprene on biogeochemical and biophysical properties, isoprene emissions are directly related to land cover [40], and so accurate land cover inputs are vital for biogenic emission models [1,2,41]. Naturally, the highest emissions of isoprene are found between the tropics over the landmass where most of the Earth's biomass is located. The isoprene fluxes from different types of vegetation are limited, and this imposes constraints on model development. The Model of Emissions of Gases and Aerosols from Nature (MEGAN) global database developed by Guenther et al. [42] with updates highlighted in Guenther et al. [2] and Sindelarova et al. [43] showed that the dominant source of isoprene emissions is broadleaf tropical forests (84.5%), followed by temperate shrubs (10%), cool and warm grass (4%), and finally needleleaf forest in boreal regions (1.5%) (Table 1). Thus, the emitted isoprene is mostly visible in the tropical region (e.g., 56% in the southern tropics and 32% in the northern tropics), followed by temperate regions (e.g., 7% in the northern temperate and 4% in the southern temperate) with a minor contribution from the northern Arctic (<1%).

Table 1. Global land area (10^{12} km^2) and isoprene emissions for individual plant functional types estimated using MEGAN2.1 algorithms for the year 2000. Adapted from Guenther et al. [2].

Plant Species	Land Area (10^{12} km^2)	Isoprene ($Tg\ yr^{-1}$)
Needleleaf Evergreen Temperate Tree	5.46	1.61
Needleleaf Evergreen Boreal Tree	10.6	5.9
Needleleaf Deciduous Boreal Tree	1.46	0.0002
Broadleaf Evergreen Tropical Tree	15.6	244
Broadleaf Evergreen Temperate Tree	2.64	21.9
Broadleaf Deciduous Tropical Tree	12.9	178
Broadleaf Deciduous Temperate Tree	5.33	35.4
Broadleaf Deciduous Boreal Tree	2.14	4.79
Broadleaf Evergreen Temperate Shrub	0.18	0.23
Broadleaf Deciduous Temperate Shrub	4.15	21.8
Broadleaf Deciduous Boreal Shrub	9.33	2.93
Arctic C3 Grass	4.94	0.97
Cool C3 Grass	14.3	11.2
Warm C4 Grass	13.2	5.93
Crop 1	16.3	0.02
Total	118.5	535

Amazonia is known to be a major source of isoprene emissions. Areas of elevated isoprene emissions can also be seen over Russia and Canada in a biome known as boreal forest. Regions of boreal forest, or Taiga, are characterized by coniferous trees situated in a highly seasonal climate, with cold seasons seeing extreme low temperatures and snow coverage. In spring, the melted snow reveals vast forests that can achieve high rates of photosynthesis and hence release a significant mass of isoprene contributing to the global budget [44]. Karl et al. [45] estimated that over 70% of total emitted BVOCs originate from the tropics, and Figure 1 shows how the south tropical region dominates the spatial distribution of isoprene emissions globally [43]. Emissions of isoprene are also strongly species-dependent, leading to further spatial differences in the distribution of emissions between distinct tropical regions such as Amazonia and Southeast Asia.

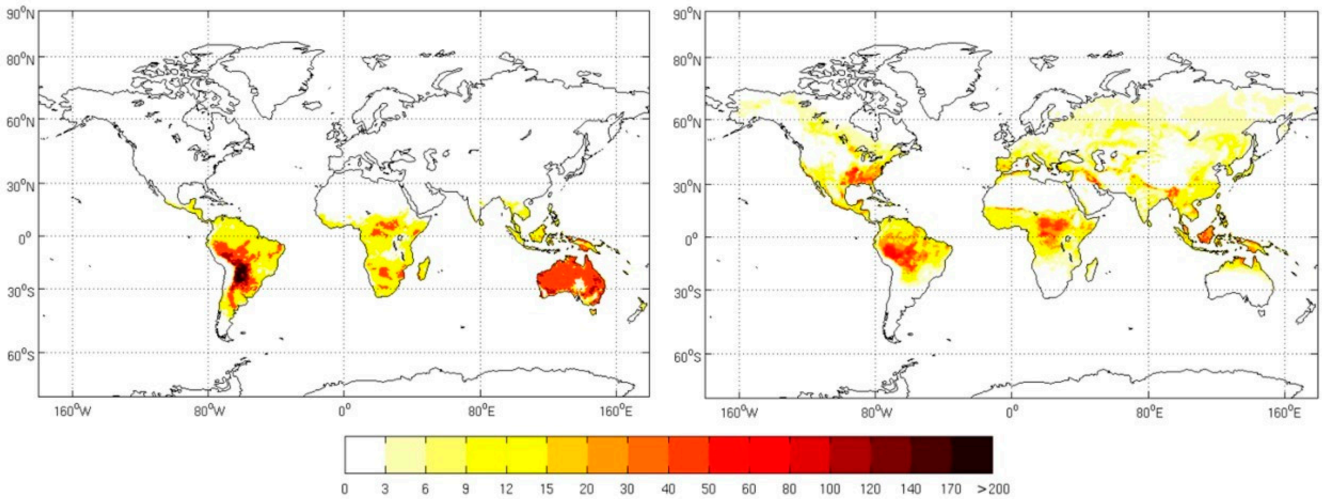

Figure 1. Spatial distribution of mean isoprene emissions (mg m^{-2} day^{-1}) for January (**left**) and July (**right**) averaged over the years 1980–2010 calculated by the MEGAN model. The figure is adapted from Sindelarova et al. [43].

Numerous field and modeling studies have calculated a value for the atmospheric emission flux of isoprene and have shown remarkably consistent results. Arneth et al. [3] summarized several previous studies to investigate why estimates of global terrestrial isoprene emissions are so similar when the same is not true for monoterpenes (another prominent BVOC). They calculated an average annual global terrestrial isoprene emission rate of 516 TgC yr^{-1}, with a range of 460–570 TgC yr^{-1}. For perspective, this estimated flux of isoprene is roughly equal to the annual atmospheric flux of methane on a carbon mass basis [1]. Atmospheric modelling by Pacifico et al. [46] estimated global annual isoprene emissions of 460 TgC yr^{-1}, and Sindelarova et al. [43] estimated emissions of 523 TgC yr^{-1}, both showing agreement with previous studies and the average range calculated by Arneth et al. [3].

The experimental data indicates that temperature and light are the key environmental factors affecting isoprene emission from plants [47]. The architecture, leaf size, and form of the existing plants all have an impact on many of these variables, which vary across the canopy. It is generally known that isoprene emission depends on light, which differentiates isoprene emissions from monoterpenes and other hydrocarbon emissions from plants that occur at night. Isoprene emissions are strongly temperature sensitive. The evaporation temperature of isoprene is very low (34 °C), which explains the exponential growth of isoprene emissions at physiological temperatures [48]. Due to the great temperature sensitivity of isoprene synthesis, the temperature is a crucial factor affecting the rate of isoprene emission. Young leaves do not release isoprene, and isoprene emission normally occurs several weeks after the start of photosynthesis at the start of the growing season. The leaves must attain complete maturity before the maximum isoprene emission rates may be reached, which in certain species may not happen until the beginning of the summer. When dealing with isoprene emissions, it is important to specify the regions, seasons, and types of plants.

In addition to temperature and light, isoprene emissions are controlled by the levels of carbon dioxide (CO_2). It was found from laboratory and field studies that a direct inhibition of isoprene production was caused by an increasing concentration of atmospheric CO_2 which can have opposite responses to surface ozone concentrations, e.g., decreases in polluted regions and increases in less polluted regions [49]. The tropical forests may have the ability to maintain a strong atmospheric oxidation capacity whilst emitting large quantities of isoprene, which may to a degree be explained by the CO_2 inhibition effect. Climate change had the potential to increase levels of isoprene emissions due to higher temperatures; however, increased concentrations of CO_2 would oppose this effect. In future climate change scenarios, including the CO_2 inhibition effectively cancelled out climate-induced increases in isoprene emissions, and modeled global isoprene emissions in 2100 could be very similar to present-day emissions [46]. A similar conclusion was reached in a study by Heald et al. [50] who also suggested that future isoprene emissions would be, to a large degree, buffered by competing influences (CO_2 inhibition effect), with the projected global isoprene emissions in 2100 dropping from 696 to 479 TgC yr^{-1}. Wilkinson et al. [51] showed that the isoprene emission rates from several species of trees (eucalyptus, sweetgum, cottonwood, and aspen) were reduced when trees were exposed to a higher concentration of CO_2 whilst growing. They presented a new model [51] for isoprene emission accounting for its response to CO_2, consistent with Guenther and co-workers' [1] algorithms, which can be used for the effect of long-term changes in CO_2 levels on isoprene emission rates. However, Sun et al. [52] showed that the CO_2 inhibition effect may not take effect in a warmer climate, as the isoprene could protect leaf photosynthetic function against heat stress more effectively under increased CO_2 levels. Furthermore, Heald et al. [50] discussed the possibility of the CO_2 inhibition of isoprene emissions being counteracted by the fertilization effect of CO_2, which enhances photosynthesis and water use efficiency, hence also increasing vegetation productivity.

Isoprene is rapidly oxidized once it is emitted into the atmosphere, leading to its breakdown and a lower overall concentration despite a high initial emission rate. Thus, an accurate representation of isoprene oxidation chemistry is of vital importance to global atmospheric models.

3. Initial Isoprene Oxidation Chemistry

Oxidation by hydroxyl radicals (OH) is the main atmospheric removal process for isoprene. Hydroxyl radicals can add to any of the four carbons involved in double bonding, as shown labeled in Figure 2. Peeters et al. [53] found experimental evidence to support (within a few percent) their structure-activity relation predictions of 60% 1-OH-, 30% 4-OH-, 5% 2-OH-, and 5% 3-OH-isoprene adducts.

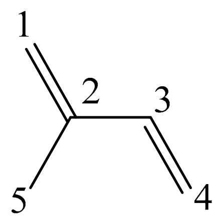

Figure 2. Structure of isoprene with C-atom labelling.

Whilst the more stable trans structure is the dominant conformer of isoprene, the addition of a hydroxyl radical releases around 38 kcal mol^{-1} of energy. The trans- and cis-structures of the activated OH-isoprene adducts are thus able to readily interconvert as suggested in the Leuven isoprene mechanism (LIM), facing barriers of only 14–15 kcal mol^{-1}. After the initial reaction between isoprene and OH radicals, peroxy radicals are formed.

Traditionally, chemical regimes have been divided into high NO_x (where the formation of peroxy radicals is the rate-limiting step for oxidation chemistry) and low NO_x (where the reactions of peroxy radicals with NO_x is the rate-limiting step for oxidation chemistry). The metric was used to assign photochemical conditions that ranged from urban/anthropologically impacted (high NO_x) to remote/pristine (low NO_x). However, as a result of emission controls, NO_x levels can be as low as a few hundred ppt [54], so one should use the term high NO_x with caution when referring to urban/remote chemical regimes.

It was previously thought that at low NO_x conditions, peroxy radicals can recombine into peroxides (Pathway I), which are removed from the atmosphere through deposition processes, resulting in reduced tropospheric OH levels and thus depleting the atmospheric oxidation capacity. At high atmospheric NO_x concentrations, the alternate pathway (Pathway II) recycles OH through reactions with NO, producing secondary tropospheric pollutants such as ozone. This additional ozone can contribute to climate change as it is an effective radiative forcing agent in the tropical troposphere.

The isoprene oxidation is directly linked to the concentrations of NO_x which is mostly released during fossil fuel combustion, with an approximate rate of 30 Tg N yr^{-1} [55] However, in forest regions, soil-biogenic NO_x emissions are also important, which can globally contribute around 12.9 $\pm$ 3.9 Tg N yr^{-1} of the total source [56]. Soil-biogenic emissions of NO_x are influenced by vegetation type, use of nitrogen-containing fertilizer, and meteorological parameters such as moisture and temperature. In pathway II, the peroxy radicals formed from the initial oxidation reaction react with NO to form NO_2. The subsequent photolysis of NO_2 produces NO and ground state oxygen atoms, which can react with O_2 to form tropospheric O_3. Barket et al. [57] showed that the oxidation of isoprene produced a significant amount of ozone with a rate of 1–5 ppb ozone per hour during daytime for the anthropogenically impacted rural environments (NO_x concentrations in the range of 0.1–10 ppb). However, the simulated impact of isoprene emissions on the global O_3 burden is small overall [46]. This is in agreement with previous studies where 91–92% of increased ozone concentrations were found to be related to direct effects of human activities [58].

The low-NO_x oxidation scheme, which is applicable to the forested and remote regions, highlights the historical controversy over isoprene oxidation mechanisms, as early mechanisms suggested a near-complete titration of isoprene. The observations of elevated OH concentrations in tropical forested regions (e.g., Amazon, Borneo) throughout the 2000s [59,60] contradicted these findings, and a large model-measurement of OH breakdown began to become apparent. Unexpectedly high OH concentrations, up to 10 times more than predicted by models at the time, were measured [61]. These differences were most noticeable in areas where high isoprene concentrations (>1 ppbv) corresponded with low NO_x concentrations (<1 ppbv). Hofzumahaus et al. [62] calculated the turnover rates of OH and HO_2 during a measurement campaign in the Pearl River Delta, China. The calculated OH concentration was found to be 3- to 5-fold higher than expected, and they proposed the additional OH was being generated by a pathway independent of NO and thus not producing additional ozone. These findings suggest that there is an unknown recycling mechanism of OH at low NO_x which is not included in conventional isoprene degradation mechanisms. Lelieveld et al. [59] suggested that an OH recycling efficiency in isoprene oxidation of 40–80% was needed to explain the unexpectedly high OH concentrations over the Amazon rainforest.

4. Isoprene HO_x Recycling and Updated Isoprene Oxidation Chemistry

The increased understanding of isoprene HO_x recycling at low NO_x has occurred in the past 15 years, mostly due to the realisation that H shift reactions in peroxy radicals formed in the initial oxidation of isoprene can occur quickly enough to compete with, or even dominate, their reactions via pathways I (attachment to the 1-carbon) and II (attachment to the 4-carbon atom) [53,63]. A theoretical study conducted by Peeters et al. [53] proposed that unimolecular isomerization reactions of specific RO_2 radical isomers by 1,6-H- and 1,5-H-shifts are sufficiently rapid to be competitive with bimolecular reactions with other peroxy radicals to form organic hydroperoxides (ROOH). The new RO_2 radicals formed from unimolecular isomerization generate additional ROOH, which can be photolyzed, leading to a significant source of OH. These HO_x regenerating reactions have subsequently been included in many atmospheric models and were estimated to yield ~0.7 HO_2 and ~0.03 OH radicals per isoprene oxidized [53]. A chamber study with conditions relevant to the remote forested regions undertaken by Paulot et al. [63] found the formation of high concentrations of dihydroxyepoxides via an OH neutral pathway. These dihydroxyepoxides are thought to be more stable (lifetime with respect to OH addition is of the order of 18–22 h) than the precursor hydroperoxides, and their reactive uptake to aerosol surfaces may lead to a significant source of isoprene-derived secondary organic aerosol (SOA). The stability of the hydroxyepoxides could also help to explain the remarkable stability of OH in remote regions, as it is a stable chain-terminating reaction formed by an OH neutral mechanism.

Due to the presence of allyl resonance in both the 1-OH and 4-OH adducts as well as the proposed isoprene oxidation mechanism [53], initial OH isoprene adducts can quickly add O_2 molecule at two additional sites, as depicted in Figure 3. The Z-δ-OH-peroxy (i.e., Z-1-OH-4-OO. and Z-4-OH-1-OO.) is demonstrated to be the most reactive in both cases. In this compound, the weakly bonded α-OH hydrogen undergoes a 1,6-H shift to the peroxy radical site to produce a resonant hydroxy hydroperoxyalkenyl radical. These radical products can react quickly with O_2 generating HO_2 along with photolabile hydroperoxyl-methylbutenals (HPALDs), which quickly produce OH radicals. In addition to the 1,6-H shift channel, the 1,5-H shift reaction of the β-OH peroxy radicals produces HO_x radicals along with oxygenated organic products methacrolein (MACR), methyl vinyl ketone (MVK), and formaldehyde [53,64]. However, the OH radical generation through 1,5-H shift is found to be very low compared with 1,6-H shift isomerization [61].

Crounse et al. [65] reported experimental evidence for the formation of HPALDs from 1,6-H shift isomerization for δ-isoprene peroxy radicals with $k_{isom}(295\ K) = 0.002\ s^{-1}$. They estimated that the fraction of isoprene peroxy radicals reacting through this mechanism could be 8–11% globally, up to 20% in the tropics. This rate is substantially slower than predicted in the theoretical calculations [53,66,67]. The direct comparison to the theoretical rate is not straightforward, as the experimental study [65] only observed the end products of interconversion between the β-OH-OO, Z-δ-OH-OO, and E-δ-OH-OO radicals and the 1,6-H shift reactions of the Z-δ-OH-OO radicals. From the isomerization rates determined, Crounse et al. [65] concluded that isomerization reactions of isoprene peroxy radicals were unlikely to explain the differences in HO_x concentrations between model measurements [68].

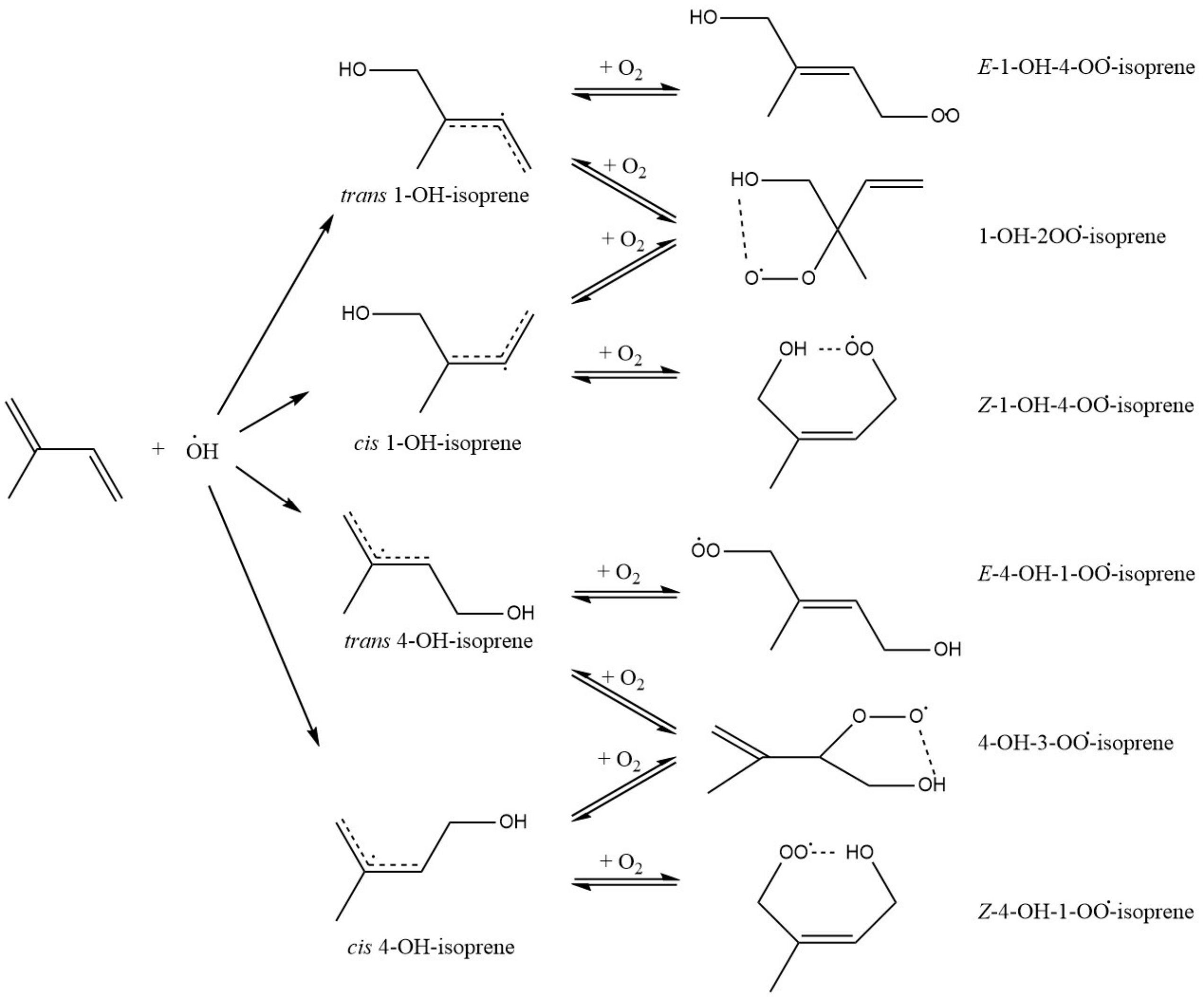

Figure 3. Reaction scheme for the addition of O_2 to initial 1-OH and 4-OH adducts of isoprene, following the reaction of isoprene with an OH radical. Adapted from Peeters et al. [53].

Archibald et al. [68] used a box model to investigate the impacts of mechanistic changes on HO_x formation and recycling in the oxidation of isoprene in remote forested regions. The Master Chemical Mechanism version 3.1 (MCM v3.1) was used as a base reference mechanism with sensitivity studies conducted over a wide range of NO_x levels. The radical propagating channels for the reactions of HO_2 with RO_2 radicals (namely acyl and β-oxoperoxy radicals) and the partial revision of the first generation hydroperoxides (representative of Paulot et al. [63] OH regeneration) in their study led to increases of OH concentrations by ~5–7% over the sub-ppb NO_x range. However, implementing the unimolecular isomerization reactions proposed by Peeters et al. [53] into the MCM mechanism yielded a factor of up to 3.3 increase in the OH concentration, with the highest increase at the low end of the NO_x range. A representation of isoprene HO_x recycling for use with the Common Representative Intermediates version 2, reduction 5 (CRI v2-R5) mechanism was developed using the MCM v3.1 sensitivity studies as a reference benchmark [68]. The mechanism included a reduced representation of HO_x recycling resulting from isomerization of isoprene-derived peroxy radicals (based on Peeters et al. [53]) and the inclusion of propagating channels for the reactions of HO_2 with acyl peroxy radicals [69]. The inclusion of isoprene HO_x recycling caused an increase of up to 40% in the OH concentration over forested regions (the tropics in February and the tropics as well as forested boreal regions in August) with an increase of more than 20% simulated in the free troposphere [68].

The theoretical study [61] showed that 1,6-H shift isomerization occurred with large reaction rate constants (5.7 s^{-1} and 0.52 s^{-1} at 298 K for 4-OH and 1-OH adducts, respectively), which are in good agreement with the experimental study (3.6 s^{-1} and 0.4 s^{-1}, respectively) [70]. However, 1,5-H shift isomerization occurred with small reaction rate constants (1.1×10^{-3} s^{-1} and 0.7×10^{-3} s^{-1} at 298 K for 4-OH and 1-OH adducts, respectively) [61], which makes the reaction competitive only in the presence of exceptionally low NO levels (<10 pptv). Peeters et al. [61] updated the isomerization mechanism (Figure 4) and suggested that the bulk isomerization of Z-δ-OH-peroxy 1,6-H-shift rate k_{isom} increases approximately linearly with the traditional bimolecular reaction rates, k_{tr}, because these bimolecular reactions reduce the abundances of majority β-OH peroxy radicals but have much less influence on the abundances of Z-δ-OH-peroxy radicals. In the experiments of Crounse et al. [65], traditional bimolecular reaction rates, $k_{tr,}$ were found to be ~0.02 s^{-1}. However, Xiong et al. [71] reported that k_{tr} is highly variable with NO_x levels with a range of ~0.02 s^{-1} in the afternoon (low NO) to ~0.1 s^{-1} in the morning (high NO). The measured bulk isomerization rate reported by Crounse et al. [65] is at the lower end of atmospherically relevant k_{tr}, which leads to an underestimation of the actual isomerization rate in their study.

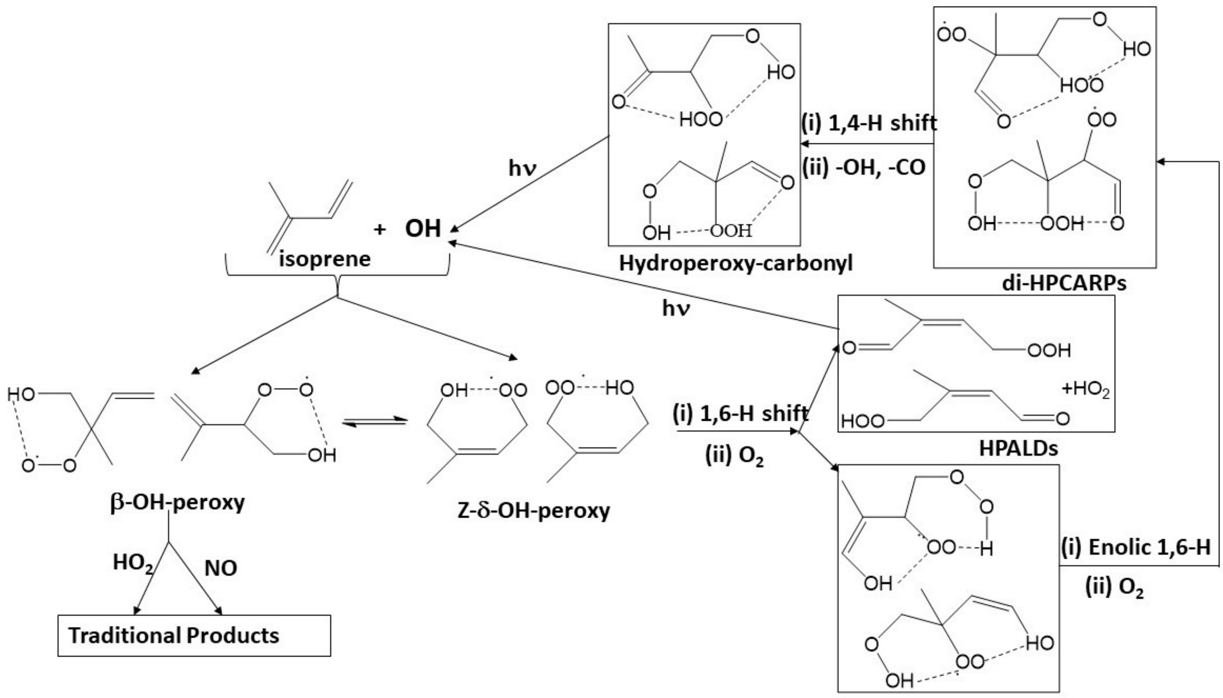

Figure 4. Updated reaction scheme of OH-initiated oxidation of isoprene under low NO_x conditions (adapted from [61]).

The addition of O_2 to the hydroxy hydroperoxyalkenyl radicals produced from 1,6-H shift isomerization of Z-δ-OH-peroxy can proceed equally via α-hydroxy H atom abstraction to yield HPALDs and HO_2 and via addition γ to the OH group, leading to the production of the complex dihydroperoxy-carbonyl peroxy radicals, di-HPCARPs (Figure 5) [61]. Under low NO_x conditions, di-HPCARPs react significantly via a 1,4-H-shift isomerization reaction to form OH, carbon monoxide (CO), and dihydroperoxy-carbonyl compound, which also photolyzes rapidly to produce additional OH.

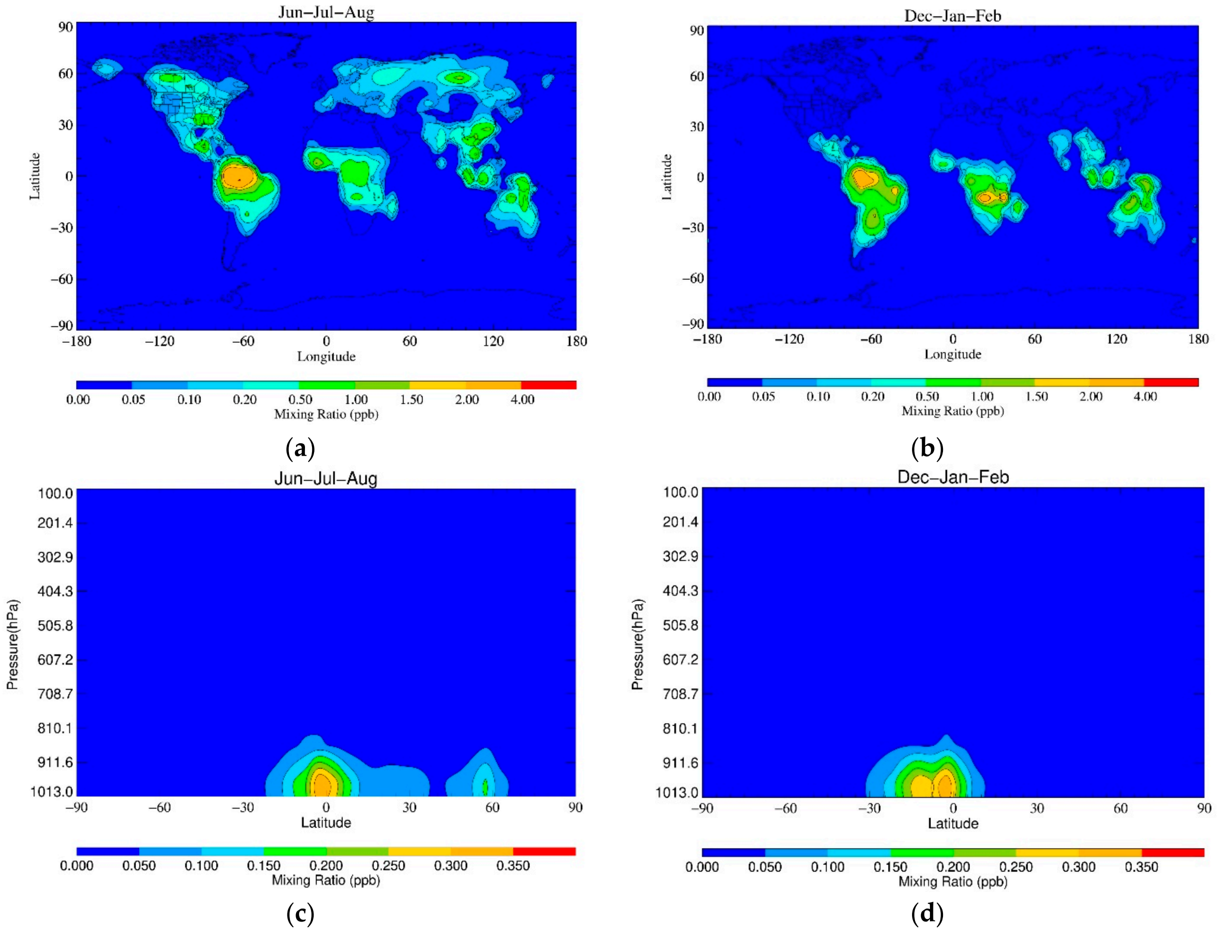

Figure 5. Mixing ratios of isoprene simulated by STOCHEM-CRI (**a**) surface distribution for June-July-August, (**b**) surface distribution for December-January-February, (**c**) zonal distribution for June-July-August, (**d**) zonal distribution for December-January-February.

There are large uncertainties on the yields of HPALD and di-HPCARPs. Peeters et al. [61] proposed a theoretical yield of ~0.5 for HPALDs and di-HPCARPs. The experimental studies conducted by Teng et al. [70] and Wennberg et al. [72] obtained a total yield of 0.4 (β-HPALD ~0.15, δ-HPALD ~0.25). Some other experimental and theoretical [73–75] studies suggested the formation of HPALDs with very high yield of ~0.75. A recent theoretical study by Szabó et al. [76] reported a δ-HPALD yield of ~1 with negligible contribution from β-HPALD. However, another recent experimental study performed by Medeiros et al. [77] indirectly determined very low HPALD yield of 0.19 without distinction between the β- and δ-isomers.

The chemistry of isoprene degradation in the MCM was refined and updated to reflect advances in understanding in the latest version, MCM v3.3.1, consisting of 1926 reactions of 602 species [78]. The updates mainly related to the OH-initiated chemistry, which has large impacts on HO_x recycling at lower NO_x levels, with particularly important simulated contributions resulting from the chemistry initiated by the 1,6-H shift isomerization reactions of the Z-δ-OH-peroxy and from the higher-generation 1,4-H shift isomerization reactions of the α-formyl peroxy radicals. The rate coefficient for the 1,6-H shift isomerization reaction is based on those reported by Peeters et al. [61] but scaled (slower by a factor of ~5) to recreate the phenomenological bulk isomerization rate (k_{bulk}) to form the HPALDs for the conditions of the experiments reported by Crounse et al. [65]. The revised oxidation chemistry of isoprene was also incorporated into the CRI v2-R5 mechanism [79] using the MCM v3.1.1 sensitivity studies as a reference benchmark.

Müller et al. [74] implemented a new chemical mechanism for the oxidation of BVOCs in the Model of Atmospheric Composition at Global and Regional Scales using Inversion Techniques for Trace Gas Emissions (MAGRITTE v1.1), incorporating the representation of isoprene's oxidation scheme with major advances in recent theoretical and laboratory studies. The isomerization reactions in the study of Müller et al. [74] controlled the fate of about one-fifth of the total flux of hydroperoxy radicals formed from the reaction between isoprene and OH (16.5% for the 1,6-H shift and 3% for the 1,5-H shift). Accurate modeling of isoprene emissions, involving the most up-to-date understanding of isoprene oxidation chemistry, would increase the understanding of the global environmental impacts of isoprene oxidation.

5. Environmental Impacts of Isoprene

Isoprene is not seen to be a major threat to human health in its unreacted form, with only unrealistically high concentrations considered carcinogenic, though it possesses a greater risk when its subsequent atmospheric reaction products are considered [80]. As isoprene is highly reactive, its double bonds make it vulnerable to attack by the nitrate radical (NO_3), OH, and O_3, with atmospheric lifetimes of 0.8 h, 1.7 h, and 1.3 days, respectively [81]. Isoprene's impact on climate, air quality, and human health can be recognized on both regional and global levels due to the persistence of long-lived multi-stage oxidation products. The oxidation normally occurs in the boundary layer in the vicinity of the emission regions, where it has a significant impact on the oxidizing capacity, the global carbon cycle and radiative forcing [82–84]. Isoprene emissions contribute to various atmospheric processes such as the formation of tropospheric O_3, affect the lifetime of methane (CH_4), and the growth of SOA, which could have important climatic impacts [19,63,85]. Calculating the impact of isoprene emissions released by plants on the atmosphere is challenging because the reactions involve radicals, can take many alternative paths, and rely on the concentrations in a highly non-linear manner.

Under high NO_x conditions ([NO_x] > 1 ppb), reactions between initial isoprene oxidation products and NO recycled HO_x led to the formation of tropospheric ozone, which is considered a major pollutant [83,86]. Under low NO_x conditions, isoprene reacts directly with O_3 and thus reduces tropospheric O_3 levels. In addition, the isoprene oxidation with HO_x recycling led to a change in the oxidative capacity of the troposphere [87]. Peroxyacetyl nitrates (PANs) can also be produced when isoprene breaks down [88], which are recognized as phytotoxins, bacterial mutagens, and eye irritants (lachrymators). Its phytotoxic biological effects, which harm plants and vegetation, are the most detrimental [89]. Some isoprene oxidation products at both high and low NO_x conditions have been identified as precursors to the formation of SOA, which influences the number of climatically relevant particles in the atmosphere.

SOA is the dominant contribution to atmospheric particulate organic matter (POM), which is highly variable with season and location, and in tropical forest regions, POM accounts for up to 90% of total atmospheric particulate mass [90]. The biogenic SOA can act as condensation nuclei for cloud droplet formation in the atmosphere, thus exerting a negative radiative effect on the climate [91]. Historically, it was thought that isoprene did not contribute to SOA formation because of the volatility of its key oxidation products, e.g., methacrolein, methyl vinyl ketone, glyoxal, methylglyoxal, glycolaldehyde, hydroxyacetone, and formaldehyde [92]. However, SOA formation from isoprene oxidation has been intensively explored during the last two decades and found that the overall contribution of isoprene to total atmospheric POM could be large (e.g., 6 Tg/yr) because of its large global emission flux [93]. The isoprene oxidation mechanisms identified specific SOA precursors such as isoprene epoxydiols (IEPOX) at low NO_x environments and methacryloyl peroxynitrate (MPAN) at high NO_x environments [94]. In isoprene-dominating regions (e.g., the Amazon rainforest), a significant amount of IEPOX can be formed, and their reactive uptake on acidic sulfate aerosols may lead to a substantial production of SOA from isoprene. SOA can directly interact with incoming shortwave radiation (a direct radiative effect) and act as condensation nuclei for cloud droplet formation (an indirect radiative effect). Considering these direct and indirect radiative effects, it is thought that SOA produced from isoprene in the atmosphere exerts a negative radiative effect on the climate [90,95]. Recent aircraft observations [96,97] showed new particle formation (NPF) from extremely low volatile oxidation products of isoprene in the Amazonian upper troposphere, which can serve as cloud condensation nuclei (CCN) and influence the Earth's hydrological cycle, radiation budget, and climate.

The incidence of the secondary products produced from isoprene oxidation processes in the troposphere increases the prevalence of respiratory diseases and damages the environment and infrastructure. Pye et al. [98] have shown that across the United States, biogenic SOA mass was comparable with anthropogenic SOA mass and showed that biogenically derived SOA played a role in cardiorespiratory disease mortality. Pacifico et al. [46] highlighted the importance of considering isoprene emissions and their impact on atmospheric chemistry and climate due to the complexity of competing influences on both emissions and the degradation mechanism of isoprene. Large emissions of isoprene, coupled with its short atmospheric lifetime, leads to difficulties in global atmospheric modelling, due to a corresponding reduction in the levels of OH over isoprene source regions.

The model simulation of the initial isoprene HO_x recycling mechanism [53,59,63,66] incorporated into the global tropospheric chemistry-transport model, IMAGESv2 [99], showed an increase of OH and HO_2 concentration by a factor of 4 and 3, respectively, over the Amazon basin and an ~8% increase of ozone over tropical forests. Archibald et al. [100] showed the impacts of initial isoprene HO_x recycling for present-day, pre-industrial and future climate/emission scenarios using UKCA global chemistry-climate model. Their calculations showed that the inclusion of unimolecular isomerizations of the isoprene hydroxy-peroxy radicals increased the production of HO_x radicals in all scenarios. For the present-day climate scenario, they showed an enhanced OH and HO_2 concentration by as much as 410% and 225%, respectively, at the surface in tropical regions and up to 75% OH in the zonal within the boundary layer of the tropics, which could be important to reproduce the high concentrations of HO_x measured in the tropics by Lelieveld et al. [59]. The inclusion of HO_x regeneration and recycling in the oxidation of isoprene in their model increased the global burden of ozone by 25 Tg (8%), 36 Tg (18%), and 32 Tg (9%) and decreased the atmospheric lifetime of methane by 14%, 35%, and 11% for present, pre-industrial, and future climate/emission scenarios, respectively.

The implementation of CRI-updated isoprene degradation chemistry into the STOCHEM-CRI chemistry transport model [79,101–103] showed an increment of the global tropospheric burdens of OH and HO_2 by 6.4% and 0.8%, respectively. The increase in HO_x did in turn reduce isoprene's tropospheric burden by ~17% and shorten its tropospheric lifetime from 2.7 days to 2.2 days [87]. The peak isoprene is found over the Amazon rainforest, southern Africa, Southeast Asia, and North Australia with levels between 1 ppb to 4 ppb as a 24 h average (Figure 5a,b). There are also substantial emissions leading to levels up to 1 ppb over North America and Russia, and because of more sunlight during June-July-August (Figure 5b), leading to greater biological production in the northern hemisphere. The zonal distribution of isoprene shows the peak at the surface in the tropical region with levels going up to 0.35 ppb during both June-July-August and December-January-February seasons (Figure 5c,d). The peak at the surface in the boreal forested regions are seen with levels up to 0.2 ppb during summer (June-July-August) season. The concentrations of isoprene decrease significantly with altitude because of its short atmospheric lifetime.

Jenkin et al. [79] showed that the isoprene HO_x recycling increased model OH levels significantly over low NO_x and high isoprene emission regions, i.e., the tropical forests (typically 15–30%) and the boreal regions over Russia and Canada (typically 5–10%) (Figure 6a). Furthermore, the updated isoprene oxidation chemistry in the STOCHEM-CRI model can reduce the lifetime of methane by 5%, increase the global burden of organic nitrates by 180%, and reduce the tropospheric ozone and methane mixing ratios by up to 10% and 0.8%, respectively, over the tropical forest region (Figure 6b,c) [87].

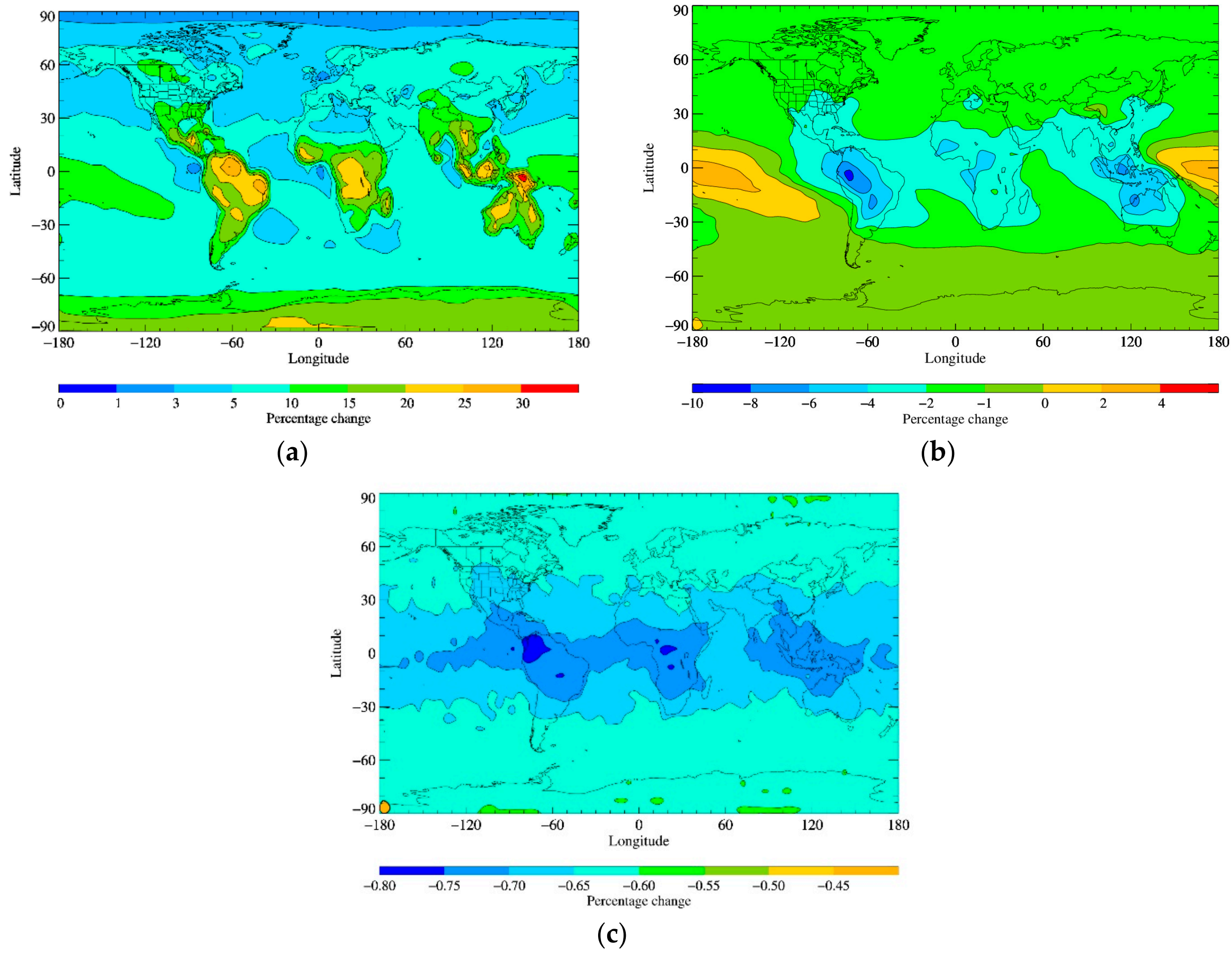

Figure 6. The percentage changes of annual surface mixing ratios of (**a**) OH, (**b**) O_3, (**c**) CH_4, simulated by STOCHEM-CRI following implementation of the isoprene HO_x recycling.

The simulation study considering the recycling of OH radicals in isoprene oxidation through the isomerization of *Z*-*δ*-hydroxyperoxy radicals in the MAGRITTE model by Müller et al. [74] showed enhanced OH concentrations by up to 40% over western Amazonia in the boundary layer and by 10–15% over the southeastern US and Siberia in July. Their study also reported that isomerization reactions led to increased HO_2 concentration by up to ~20% and reduced isoprene nitrate formation by up to ∼40% over Amazonia. Bates and Jacob [82] also discussed the hydrogen shift reactions throughout the isoprene oxidation mechanism and used the condensed version of the reduced Caltech isoprene mechanism (RCIM) [73]. Using a global GEOS-Chem model simulation with RCIM, they estimated that the fraction of isoprene reacting with OH globally (88%) and the resultant hydroxy-peroxy radicals react with HO_2 (44%), NO (28%), and RO_2 (9%) or undergo H shifts to regenerate

HO_x (22%). Bates and Jacob [82] looked at the overall effect of including updated isoprene chemistry, noting an increase in OH recycling, which, under low NO_x conditions, resulted in a lower depletion of OH than reported in previous mechanisms. They calculated that the presence of isoprene in the atmosphere could be responsible for an 11% decrease in OH, 6.5% increase in HO_2, 4.2% decrease in NO_x over the troposphere, and the increased OH resulted in a 12% increase in the tropospheric lifetime of methane. They also found that the updated isoprene oxidation chemistry could increase tropospheric ozone by 1.9 ppbv but decrease ozone levels by as much as 3.4 ppbv over tropical forest regions. The study also estimated the total global source of SOA from isoprene of 61 TgC yr^{-1} (136 Tg yr^{-1}), with approximately equal contributions from IEPOX, organonitrates, and highly functionalized C_5 compounds.

However, a recent study [104] developed a new mechanism, CRI-HOM, incorporating it into the global chemistry-aerosol-climate model to simulate the formation of highly oxygenated organic molecules (HOMs) from the oxidation of α-pinene. The simulation with the inclusion of CRI-HOM showed a significant impact of isoprene-driven suppression of involatile biogenic-derived species and the consequences for SOA.

Evaluating the models against atmospheric measurements of isoprene is required to determine the extent to which using an updated isoprene oxidation mechanism improves or reduces the accuracy of the model. The amount of isoprene measurement data from surface stations has increased enormously over the last thirty years, which is beneficial to evaluate the model simulations.

6. Measurements of Isoprene and Model Validation

The short lifetime (typically from minutes to hours [105]) results in isoprene concentrations being localized to emission regions, thus increasing the spatial and temporal range of measurements, which is important for better understanding its sources, sinks, and atmospheric impacts on local, regional, and global scales. However, *in-situ* measurements of isoprene are sparse and limited due to logistical difficulties. Early studies most commonly utilized a technique where isoprene was collected in cartridges, and these field samples were transported outside of Amazonia to be analyzed by gas chromatography techniques, e.g., Gas Chromatography-Flame Ionization Detection (GC-FID), Gas Chromatography-Mass Spectrometry (GC-MS) [106]. Whilst the development of new sampling approaches (e.g., use of drones) and more advanced analytical tools (proton-transfer-reaction mass spectrometry (PTR-MS), comparative reactivity method, photoionization detector (PID), semi-volatile thermal desorption aerosol gas chromatography) has meant that the emission of isoprene has been more easily measured on site in recent years. Table 2 shows a summary of isoprene's measurement techniques, measurement location, and measured as well as modeled mixing ratios for different campaigns.

Table 2. Measured isoprene mixing ratios, measurement techniques, and the modeled isoprene mixing ratios at different locations.

Location	Time	Lat, Lon	Measurement Technique	Measured Isoprene Mixing Ratio (ppb)	Modeled Isoprene Mixing Ratio (ppb)
Canada, Egbert [107]	Jul	44, −79	GC-FID	0.5	0.18
Canada, Kejimkuijik [107]	Jul	45, −65	GC-FID	2.0	0.13
Canada, Fraserdale [108]	Jul–Aug	50, −82	GC-FID	0.5–5	0.20
Alabama, USA [109]	Jun–Jul	32, −88	GC-FID	3.8	1.61
Michigan, USA ~801 m [110]	Aug	45, −85	GC-MS	1.36 *	0.18
Colorado, USA ~2840 m [111]	Jun–Aug	39, −105	GC-FID	0.15 ± 0.10 *	0.06
North Carolina, USA ~1100 m [112]	Jun–Jul	36, −82	GC-MS/FID	0.74 ± 0.58 *	0.38
Nevada, USA ~1315 m [113]	Jun-Sep	38, −120	GC-FID	0.397 ± 0.558 *	0.06
Amazon Basin, Brazil [114]	Jul	−2, −60	GC-FID/PID	2.2 (1.2–3.2)	2.55
Amazon Basin, Brazil [115]	Annual	−2, −60	GC-FID	2.4 (1.0–5.2)	2.13
Amazon Basin, Brazil [116]	Jul–Aug	−2, −60	GC-FID	2.0 (1.1–2.7)	2.53
Central Amazonia, Brazil [117]	Dec–Jan	−2, −60	PTR-MS	1.66 ± 0.9	2.00
Central Amazonia, Brazil [117]	Sep–Oct	−2, −60	PTR-MS	2.68 ± 0.9	1.45
Balbina, Central Amazonia, Brazil [118]	Apr	−1, −59	GC-MS	6.55 ± 1.26	2.29
Manaus-Amazonas, Brazil [45]	Sep	−2, −60	PTR-MS	7.8 ± 3.7	1.64
Manaus-Amazonas, Brazil ~1200 m [45]	Sep	−2, −60	GC-MS	5.5 ± 2.6	0.72
Manaus-Amazonas, Brazil [119]	Sep	−2, −60	PTR-MS	5.22 ± 1.5	1.64
Manaus-Amazonas, Brazil [119]	Feb–Mar	−2, −60	PTR-MS	1.5 ± 0.78	1.95
Manaus-Amazonas, Brazil [120]	Jul	−2, −60	GC-FID	3.4 ± 1.8	2.55
Central Amazonia, Brazil [121]	Sep–Nov	−2, −60	PTR-MS	5.9 ± 1.3	1.34
Central Amazonia, Brazil [121]	Dec–Feb	−2, −60	PTR-MS	5.2 ± 1.5	1.93
Central Amazonia, Brazil [121]	Mar–May	−2, −60	PTR-MS	4.1 ± 0.7	2.61
Central Amazonia, Brazil [121]	Jun–Jul	−2, −60	PTR-MS	3.4 ± 0.2	2.71

Table 2. *Cont.*

Location	Time	Lat, Lon	Measurement Technique	Measured Isoprene Mixing Ratio (ppb)	Modeled Isoprene Mixing Ratio (ppb)
Peru (~2 m) [122]	Jul	−5, −77	GC-MS/FID	3.3	0.83
Peru (91 m -1.2 km) [122]	Jul	−5, −77	GC-MS/FID	1.4	0.48
Venezuela, Buja [123]	Sep	9, −62	GC-FID	3.3	0.96
Venezuela, Auyantepuy [123]	Apr	6, −62	GC-FID	1.6	0.83
Venezuela, Calabozo [124]	Sep–Oct	9, −67	PTR-MS	0.8 (0.2–3.1)	1.40
Venezuela, Calabozo [124]	Mar–Apr	9, −67	PTR-MS	0.5 (0.1–1)	0.38
Venezuela, Parupa [124]	Jan–Feb	6, −62	PTR-MS	0.5 (0.1–1.2)	0.48
Surinam (PBL) [125]	Mar	2 to 7, −54 to −58	PTR-MS	3.5 (0.5–7)	0.87
Australia, Sydney [126]	Feb–Mar	−34, 151	PTR-MS	0.76(0.09–7.1)	0.15
Australia, Sydney [126]	Apr–May	−34, 151	PTR-MS	0.63(0.01–4.63)	0.12
Australia, Wollongong [126]	Dec–Feb	−35, 151	PTR-MS	0.28 (0.002–4.6)	0.14
Australia, New South Wales [126]	Nov	−36, 148	PTR-MS	0.15 (0.02–1.01)	0.09
Borneo, Malaysia ~426 m [127]	Apr–May and Jun–Jul	4, 117	GC-FID	1.06 (0.05–2.47)	0.66
Borneo, Malaysia ~426 m [128]	Jun–Jul	4, 117	PTR-MS	1.4 ± 1.2	0.42
Jimei District, Xiamen City, China [129]	Aug	24, 118	GC-MS/FID	0.66 ± 0.50	0.10
Jimei District, Xiamen City, China [129]	Sep	24, 118	GC-MS/FID	0.14 ± 0.21	0.09
Shanghai, China [130]	Apr–Sep	31, 121	UV-DOAS	0.22 ± 0.20	0.02
Nanjing, China ~1690 m [131]	Jul–Aug	24, 112	GC-MS	0.38 ± 0.05	0.01
Nanjing, China ~1690 m [131]	Jul–Aug	24, 112	GC-MS	0.29 ± 0.03 *	0.01
Shenzhen, China [132]	Aug–Sep	22, 113	PTR-MS	0.75	0.51
Taipei, China [133]	Jul–Aug	25, 121	GC-MS/FID	1.26	0.20

Table 2. *Cont.*

Location	Time	Lat, Lon	Measurement Technique	Measured Isoprene Mixing Ratio (ppb)	Modeled Isoprene Mixing Ratio (ppb)
Guangdong, China ~1000 m [134]	Annual	23, 112	GC-MS	0.76 ± 0.50	0.27
Hong kong ~507 m [135]	Jun–Jul	22, 114	GC-FID	1.03 ± 0.03	0.66
Lin'an Station, China ~130 m [136]	Apr–May	30, 120	GC-MS/FID	0.55 ± 0.52	0.37
Jianfeng Mountain, China ~820 m [136]	Apr–May	18, 108	GC-MS/FID	0.40 ± 0.39	0.39
Tengchong Mountain, China ~1960 m [136]	Apr–May	24, 98	GC-MS/FID	0.08 ± 0.16	0.14
Tengyue Town, China ~1660 m [136]	Apr–May	25, 98	GC-MS/FID	0.13 ± 0.06	0.06
Tai O, Hong Kong ~80 m [137]	Annual	22, 114	GC-MS/FID	0.37 ± 0.16	0.27
Mt. Tai ~1532 m [138]	Jun–Jul	36, 117	GC-MS/FID	0.15 ± 0.18 *	0.01
Tibet, China ~3816 m [139]	Jul–Aug	36, 101	GC-FID/ECD/MS	0.13 ± 0.29 *	0.01
France ~650 m [140]	Jun	43, 5	PTR-MS	2.09	0.11
Bosco Fontana Nature Reserve, Italy [141]	Jun–Jul	45, 10	PTR-MS	1.07 ± 0.80 *	0.09
Montseny, Barcelona, Spain ~720 m [142]	Jul–Aug	41, 2	PTR-MS	0.43	0.17
Ocean: Cape Town to Crozet Island [143]	Dec	−35 to −47, 18 to 51	GC-PID	0.033 *	0.0002
Ocean: Hobart to Punta Arenas [143]	Jan–Feb	−43 to −72, 147 to −127	GC-PID	0.047 *	0.002
Ocean: Punta Arenas to Cape Town [143]	Mar	−34 to −46 −71 to 18	GC-PID	0.038 *	0.032

Note: The values are reported as daytime average mixing ratios except the values with *, which are daily average mixing ratios. The sampling heights (where available) are also shown in the site description.

The isoprene mixing ratios in the Amazonian ecoregion are comparatively higher than in any other region and show an enormous variation depending on site, height, and season (Table 2). The measured isoprene mixing ratios in the Amazon follow a clear diel pattern as a function of light and temperature [117,119,120]. Compared with the dry season, a factor of two to three reduction in isoprene mixing ratios was observed at the Amazon forest during the wet season due to fluctuations in light, temperature, and leaf area index [117,119,121]. The isoprene measurements in the tropical savanna atmosphere [123,124] showed the higher mixing ratios in woodland savanna and large vegetation compared with grassland savanna and low vegetation. A seasonal cycle with lower mixing ratios of isoprene during the dry season was observed due to a lower physiological activity of the vegetation compared with the wet season [123,124]. The first airborne isoprene measurements over the tropical rainforest of Surinam by Warneke et al. [125] showed that the mixing ratios of isoprene increase strongly with the time of day and distance from the coast in accordance with ground-level emissions during the daytime. Measurements of isoprene within a Southeast Asian tropical rainforest by Jones et al. [127] showed good agreement between surface and aircraft measurements of boundary layer isoprene levels above this natural rainforest, suggesting that, at least for the region studied, ground-level observations could be treated as broadly representative of isoprene emissions for that region. Acton et al. [141], Seco et al. [142], and Kalogridis et al. [140] observed high isoprene mixing ratios at Bosco Fontana Nature Reserve, a mixed oak and hornbeam forest in northern Italy, and an elevated (720 m a.s.l.) holm oak Mediterranean forest site near the metropolitan area of Barcelona, and a French Mediterranean oak forest, respectively, during summer months due to the increased physiological activity and emission rates of the vegetation. Isoprene mixing ratios measured at US forests, e.g., Blodgett Forest, Nevada; Manitou Experimental Forest Observatory, Colorado; and PROPHET site, University of Michigan Biological Station, are impacted by local isoprene emissions from oak forests and woodlands, ponderosa pine, and quaking aspen, respectively [110,111,113]. In a recent study, Ferracci et al. [143] used the iDirac, an autonomous portable gas chromatograph coupled with photoionization detection (GC-PID), and measured high isoprene concentrations (over 500 ppt) across the Southern Ocean during summertime, indicating the marginal ice zone is a significant source of isoprene at high latitudes. The measurements of isoprene at urban (summer and autumn), coastal suburban (summer), and inland forest (late spring) sites in southeast Australia showed 3-fold and 5-fold higher isoprene mixing ratios at urban sites compared with coastal suburban and inland forest sites, respectively [126]. Significant variations in isoprene mixing ratios across different environmental regions in China are observed, e.g., (a) mountain sites in Nanjing (summer: 0.38 ppbv) [131], Guangdong (annual: 0.76 ppbv) [134], Yunnan (spring: 0.08 ppbv), Hainan Island (spring: 0.40 ppbv), and Shandong (summer: 0.15 ppbv) [138], (b) urban sites in Shanghai (summer: 0.20 ppbv, autumn: 0.20 ppbv) [130], Shenzhen (summer: 0.75 ppbv) [132], Taipei (summer: 1.26 ppbv) [133], Tengchong (spring: 0.13 ppbv), (c) coastal sites in Xiamen (summer: 0.66 ppbv, autumn: 0.14 ppbv) [129] and Lantau Island (annual: 0.37 ppbv) [137], (d) rural site in Lin'an (spring: 0.55 ppbv) [136].

There are relatively few observational studies (Table 2), which makes it difficult to develop a completely accurate model representation of isoprene's emissions and its oxidation chemistry, especially when considering regional variability. An alternative indirect approach satellite-based constraints employ is isoprene's oxidation product formaldehyde (HCHO), and this has been used over the last decade to provide top-down constraints on regional and global isoprene emissions and assess their seasonal and inter-annual variability [144–151]. However, this approach is affected due to myriad other sources of HCHO and spatial smearing in the isoprene-formaldehyde relationship. Stressed conditions, e.g., drought, can induce a large reduction in isoprene emissions, but the satellite HCHO columns did not reflect this reduction in isoprene emissions due to severe drought in the Missouri Ozarks region [152,153]. The lack of HCHO column response can be attributed to a photochemical feedback whereby reduced isoprene emissions due to the drought increase the oxidative capacity of the atmosphere, which enhances the production of HCHO from other VOCs [153]. Furthermore, the chemical link between HCHO and isoprene is a strong nonlinear function of NO_x, with the prompt yield increasing by a factor of 3 (from 0.3 to 0.9 ppbv ppbv^{-1}) over a range of NO_x values (0.1 to 2 ppbv) and background HCHO increasing by a factor of 2 (from 1.6 to 3.3 ppbv) [154]. Inclusion of the relationship of HCHO column and isoprene emission into the chemistry transport model (CTM) produced large error of the isoprene emissions with the range of 40–90% under relatively low-NO_x conditions typical of the tropics [155]. In addition, the isoprene HO_x recycling led to a decrease in the lifetime of isoprene, resulting in an increase in the ratio [HCHO]/[isoprene] by up to 50% over the tropical forest region [82,87]. Thus, using satellite measurements of HCHO as a proxy for isoprene emissions could lead to large uncertainties in isoprene concentration estimates, depending on the background conditions. Fu and co-workers [156] developed the first direct retrieval of global isoprene using Cross-track Infrared Sounder (CrIS) satellite data, which was built upon by Wells et al. [157,158] using machine learning approaches to improve sensitivity and spatial resolution. Such an approach has been used to determine isoprene emissions over large ecosystems such as tropical rainforests for daily, seasonal, and interannual variability, which can highlight the processes controlling isoprene abundance and the drivers of variability over time. However, CrIS retrievals contain no information about the diurnal profile of isoprene and only provide a snapshot at 13:30. The emission of isoprene is significant in the afternoon, and the shape/peak of the diurnal profile depends on season and location [124], which cannot be captured by current spaceborne approaches.

Comparison of the model and measurements of isoprene concentration of the sites near the strong source region (e.g., vegetation) is problematic because of the coarse model grid and small-scale horizontal variations in its concentration. Given the short lifetime of isoprene and the large model emission grids, the model produces a realistic concentration of global isoprene levels (Figure 5). The ensemble of model-measurement data presented in Table 2 gave a general evaluation of the regions featured. A disagreement between model and measured isoprene concentration with the median bias of −0.36 ppb for all campaigns is found. The observed bias is most probably due to the use of the MEGAN emission inventory, where errors in land cover and meteorological driving variables lead to a factor of 2 uncertainty [2]. The BVOC emissions algorithm in MEGAN parameterizes isoprene emission rates as a vegetation-specific standard rate, which is adjusted by scaling factors that depend on meteorological and environmental driving variables, e.g., temperature, sunlight, leaf area index, leaf age, and soil moisture. The MEGAN isoprene emissions are strongly dependent on the accuracy and resolution of the meteorology and land cover inputs [159,160]. Model performance is found to be good when accurate driving variables are used [161–164], but significant sources of uncertainty still remain: for example, given the variety of plant species, the parameterizations will not match every species present but be a representation of the class as a whole. This highlights that whilst the chemistry of isoprene oxidation is now more thoroughly understood, the uncertainty of the emission inventory is still high.

Deforestation through either direct human impact or climate change can decrease the emissions of isoprene as well as consequent environmental impact but can contribute to global climate change through the release of stored carbon, contributing to the rise in atmospheric CO_2. Understanding the potential effects of deforestation and future reforestation scenarios on the climate is important in shaping CO_2 mitigation approaches, strategy, and policy.

7. Deforestation and Reforestation and Their Environmental Impacts

Deforestation has increased over time due to the pressure of population growth, which can have a significant impact on isoprene emissions. The world's temperate zones experienced high rates of deforestation throughout the nineteenth and twentieth centuries; however, in contrast, the tropics did not see deforestation on this scale until after 1950. Rates of deforestation in the tropics reached 12 million hectares per year in the 1990s [165], before beginning to slow slightly in the twenty-first century. The overall rate of deforestation in the tropics is still approximately 9 million hectares per year, with the exception being in Amazonia, where deforestation rates have declined by nearly 80% since a peak in 2004, and an increase in planted forests (reforestation) is helping to offset the overall rate of deforestation. Scott et al. [166] showed that the simulated global deforestation can reduce isoprene emissions by 87%: most of the reduction in emissions (72%) is occurring from tropical deforestation.

There has been an increasing amount of evidence to support observations that show that, in temperate and tropical regions, the surfaces of forests are cooler than grasslands and croplands in these regions. A recent analysis, carried out by Novick and Katul [167] identified that the cooling effect on surface temperature in temperate forests also, albeit to a lesser extent, cools the air. Cooling was found to be of the order of 0.5 to 1 °C at the annual timescale, and, during the daytime growing season periods, a significantly greater effect was observed, with cooling between 2 and 3 °C.

Land cover and temperature have long been theoretically linked, which is recognized and incorporated into climate models [168–170]. Deforestation often causes increased atmospheric CO_2, which results in a positive radiative effect on the climate (i.e., the climate warms). However, forests are darker in color than grass or croplands, and so their albedo (the reflectivity of the land surface) is increased with deforestation, thus producing a negative radiative effect [166]. Overall, the balance of these impacts tends to mean that the climates of tropical forests are warmed by deforestation, whereas forests at high latitudes are cooled [171–173]. In the tropics, this can be explained by relatively large evapotranspiration [174], whilst in temperate regions, albedo-driven warming is outweighed by the combined surface temperature-reducing effects of evaporative cooling and emitted longwave radiation [175].

Models by Scott et al. [166] looked at the effects of complete global deforestation and found that this could lead to a net global warming of 0.8 °C after 100 years. In their simple scenarios, tropical deforestation contributed 0.6 °C to this warming; however, boreal deforestation cooled the climate by around 0.3 °C. In addition, deforestation can reduce ozone and SOA formation, as the loss of vegetation results in lower isoprene and other biogenic VOC emissions and can contribute to global warming. Scott et al. [166] also investigated the effect of reduced isoprene emissions on SOA and found the reduction of SOA production by 91%, with the majority of this global reduction being accounted for by tropical deforestation accounted (80%).

The paper published by Bastin et al. [176] estimated that by 2050, the global potential canopy cover (where "canopy cover" refers to an area of land that is covered by tree crown vertically projected to the ground) could shrink by as much as 223 million hectares. The majority of this loss is projected to occur in the tropics. The study also stated how over 50% of global reforestation potential could be found in just 6 countries: Russia, the United

States, Canada, Australia, Brazil, and China. Under the current climate, Bastin et al. [176] estimated that in total, 4.4 billion hectares of canopy cover could be supported on land. When cropland and urban regions are excluded, this means that there is space for an extra 0.9 billion hectares of canopy cover than currently exists (Figure 7), as calculated based on the European Space Agency's land cover model [177].

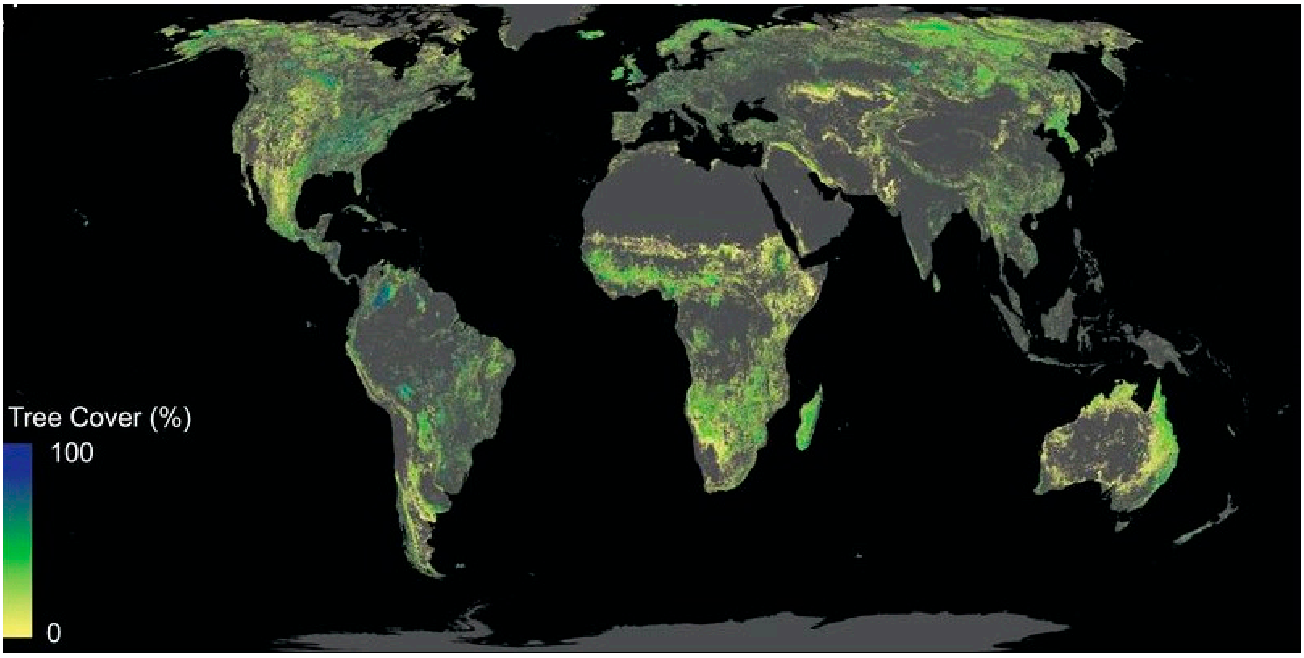

Figure 7. Global distribution of 0.9 billion hectares of extra canopy cover, which could exist outside of cropland and urban regions, based on the European Space Agency's land cover model [177]. The figure is adapted from Bastin et al. [176].

The paper by Bastin et al. [176] has been interrogated, related to calculations of the carbon storage potential of these 0.9 billion hectares of extra canopy cover (reported at 205 GtC). This carbon capture estimate represents a value 20 times that of the current annual fossil fuel emissions and a third of total historical anthropogenic carbon emissions [178]. The 205 GtC figure also seems to ignore carbon that is currently stored in these regions [179], and thus greatly overestimates the carbon storage potential of the extra canopy cover. The uncertainty over how much potential future reforestation may affect carbon sequestration continues to motivate research, but there is also great interest in whether reforestation can mitigate temperature conditions and offer a direct global cooling effect. As well as reforestation having a direct impact on the world's climate through land cover, there is also an indirect impact (e.g., oxidizing capacity of the atmosphere, increased SOA, and ozone formation) through the resulting increase in isoprene emissions.

A preliminary study of climate change due to global deforestation and reforestation have been investigated by assuming 50% reduction and 100% increase of isoprene emissions in the STOCHEM-CRI model, respectively. Decreased isoprene emissions due to deforestation lead to enhanced OH levels (Figure 8a), whereas increased isoprene due to reforestation leads to more OH depletion over the tropical forested regions (Figure 8b) in the isoprene source regions. There is a tipping point in isoprene chemistry where OH recycling peaks and then starts to decrease as more isoprene is added and commensurately less OH is regenerated, which needs to be investigated further. The formation of ozone is found to be reduced in the deforestation scenario (Figure 8c) due to the decreased peroxy radicals formed from the oxidation of isoprene with OH. The ozone is also decreased in the tropical forested region for the reforestation scenario (Figure 8d) which is due to the increased organic peroxides (ROOH) formation with increased RO_2 and HO_2. However, the increased NO_x over the equatorial oceans combined with high levels of water vapor results in an increase in ozone by up to 30% (Figure 8d). The increase of OH due to deforestation can decrease CH_4 levels in the forested region by up to 0.2% (Figure 8e), which is very small, so deforestation does not have any overall environmental impact in terms of the decreased lifetime of CH_4. However, the decrease of OH due to reforestation can increase CH_4 levels throughout the globe by up to 1% (Figure 8f), which can have an environmental impact in terms of global warming potential (GWP).

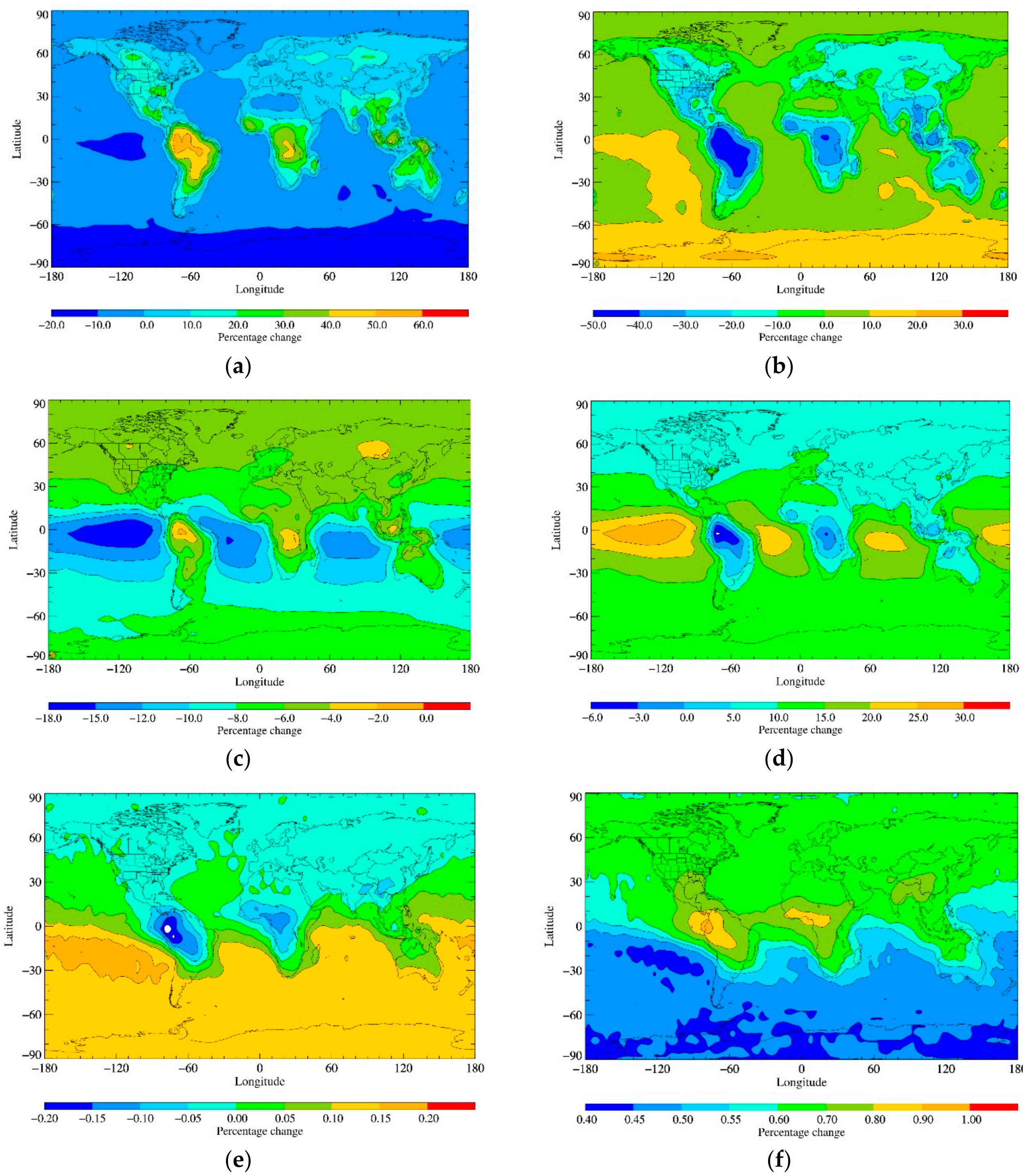

Figure 8. The percentage changes of annual surface mixing ratios of (**a**) OH, (**c**) O_3, (**e**) CH_4, simulated by STOCHEM-CRI following 50% reduced isoprene emissions, and (**b**) OH, (**d**) O_3, (**f**) CH_4 simulated by STOCHEM-CRI following 100% increased isoprene emissions.

With the high uncertainty of the isoprene emission inventory, it may be asked why research into the environmental significance of isoprene is so important. Future changes in climate and land use might lead to substantial changes in the biogenic isoprene emission, which would further influence the radiative balance in the global climate as well as the air quality in urban areas. Isoprene is integral in the formation of ozone and aerosols [83], both of which pose serious health concerns and negative environmental impacts. If the triggers to isoprene release were known, conclusions could be drawn about how the changing atmosphere could be damaging to plants, and in turn humans, through isoprene's atmospheric reactions. The impacts of deforestation could be understood from an atmospheric composition viewpoint, as well as the effect of planting large quantities of certain plant species in specific areas. Of course, a better understanding of the relationship between vegetation and atmospheric makeup would allow the estimates to be more accurate, the benefits of which would be substantial in terms of future planning, risk analysis, and environmental impact examinations.

8. Conclusions

Terrestrial vegetation accounts for a large portion of non-methane VOCs emitted into the atmosphere, with isoprene (C_5H_8) having the largest emission flux. The dominant source of isoprene emissions are broadleaf tropical forests (84.5%), followed by temperate shrubs (10%), cool and warm grass (4%), and finally needleleaf forest in boreal regions (1.5%). In both polluted and unpolluted environments, isoprene emission and oxidation chemistry can affect the climate in several ways. In the atmosphere, isoprene is oxidized by OH radicals, and isoprene can thus deplete the oxidizing capacity of the atmosphere. This causes concern as reaction with OH is also the main removal process for many other organic compounds, such as methane, which is a primary greenhouse gas (GHG). Furthermore, in polluted environments, isoprene can contribute to the production of tropospheric ozone, which is a pollutant and major component of smog. In unpolluted environments, certain isoprene oxidation products have been identified as precursors to the formation of secondary organic aerosol, which influences the number of climatically relevant particles in the atmosphere. Initial isoprene oxidation mechanisms were thrown into doubt, as far greater levels of HO_x radicals were measured over pristine Amazon rainforests than predicted by models at the time. Following the observation of this model-measurement breakdown, it was realized that the peroxy radicals formed in the initial oxidation of isoprene could undergo isomerization reactions. These 1,6- and 1,5-H shifts were found to occur fast enough to compete with, or even outperform, other isoprene oxidation pathways and isoprene oxidation mechanisms were subsequently updated. Updated isoprene chemistry has since been included in numerous studies and has reduced the model-measurement breakdown seen in HO_x concentrations. Due to the role of HO_x radicals in the oxidizing chemistry of the atmosphere, these revisions have also affected the tropospheric burdens of important species such as carbon monoxide, secondary organic aerosols, PANs, methane, and ozone. With the updated isoprene oxidation chemistry scheme, the modelled-measured isoprene concentrations are still found to be a disagreement possibly due to the uncertainty of the MEGAN emission inventory used in the STOCHEM-CRI model. Laboratory studies have enabled us to develop a full reaction scheme for the oxidation of isoprene as a function of NO_x. Such laboratory studies have revealed previously unknown pathways, such as the isomerization reactions, which have been shown to have major impacts on the oxidizing capacity of the troposphere. Whilst these studies have provided a fundamental understanding of the reaction mechanism, there still remain many unknowns. For example, there have, as of yet, not been any isomer-specific studies on the 6 peroxy radicals shown in Figure 4, and thus their fate remains highly uncertain. Chemical synthesis of novel precursors to generate one peroxy radical at a time in the laboratory are needed or to be able to measure each isomer independently in a measurement system. This would enable new experimental studies, analogous to the use of 1,1-diodo compounds as photolytic precursors of Criegee intermediates, to study their fate for the first time [180–182].

Isoprene emissions and their response to deforestation and reforestation have been a major topic studied by atmospheric chemists over recent decades. This demonstrates the need for including a correct mapping of land covers by trees due to deforestation/reforestation in models. How isoprene emissions will change in response to climate change remains highly uncertain, and thus how altered isoprene emissions will impact air quality, human health, and climate change in the future remains unknown. Coordinated field studies are required both on a local and regional scale to investigate the impact of isoprene chemistry. Isoprene emissions vary with season, diurnally and are strongly tied to temperature, water availability and light. One could imagine using the airborne Hyperspectral Thermal Emission Spectrometer (HyTES) to retrieve canopy temperature and evapotranspiration, the Airborne Visible/Infrared Imaging Spectrometer (AVIRIS) to retrieve plant functional type, and solar-induced fluorescence to retrieve GPP (gross primary productivity) in conjunction with isoprene measurements in order to improve understanding of factors controlling isoprene emissions. There is a pressing need for both long-term and diurnal measurements, which can be achieved by using multiple field campaigns in conjunction with geostationary spaceborne retrievals.

Author Contributions: M.A.H.K., C.M. and C.J.P. wrote the paper; M.A.H.K. and R.H. performed the model simulation and investigated the model data. D.E.S. and M.A.H.K. conceived and designed the project; D.E.S., R.H., C.J.P., A.B. and M.A.H.K. reviewed and edited the manuscript. All authors have read and agreed to the published version of the manuscript.

Funding: We thank NERC (NE/K004905/1; NE/J009008/1; NE/I014381/1; NE/P013104/1), Bristol ChemLabS, and the Primary Science Teaching Trust, under whose auspices various aspects of this work were supported.

Institutional Review Board Statement: Not applicable.

Informed Consent Statement: Not applicable.

Data Availability Statement: No new data were created in this study. Data sharing is not applicable to this article.

Acknowledgments: We thank Bristol ChemLabS and the Primary Science Teaching Trust, under whose auspices various aspects of this work were supported. C.J.P.'s work was carried out at Jet Propulsion Laboratory, California Institute of Technology, under contract with the National Aeronautics and Space Administration (NASA, 80NM0018D0004). and was supported by the Upper Atmosphere Research and Tropospheric Chemistry Programs.

Conflicts of Interest: The authors declare no conflicts of interest.

References

1. Guenther, A.; Hewitt, C.N.; Erickson, D.; Fall, R.; Geron, C.; Graedel, T.; Harley, P.; Klinger, L.; Lerdau, M.; McKay, W.A.; et al. A global model of natural volatile organic compound emissions. *J. Gephys. Res. Atmos.* **1995**, *100*, 8873–8892. [CrossRef]
2. Guenther, A.B.; Jiang, X.; Heald, C.L.; Sakulyanontvittaya, T.; Duhl, T.; Emmons, L.K.; Wang, X. The Model of Emissions of Gases and Aerosols from Nature version 2.1 (MEGAN2.1): An extended and updated framework for modeling biogenic emissions. *Geosci. Model Dev.* **2012**, *5*, 1471–1492. [CrossRef]
3. Arneth, A.; Monson, R.K.; Schurgers, G.; Niinemets, Ü.; Palmer, P.I. Why are estimates of global isoprene emissions so similar (and why is this not so for monoterpenes)? *Atmos. Chem. Phys.* **2008**, *8*, 4605–4620. [CrossRef]
4. Sharkey, T.D.; Yeh, S. Isoprene Emission from Plants. *Annu. Rev. Plant Physiol. Plant Mol. Biol.* **2001**, *52*, 407–436. [CrossRef]
5. Delwiche, C.; Sharkey, T. Rapid appearance of 13C in biogenic isoprene when $^{13}CO_2$ is fed to intact leaves. *Plant Cell Environ.* **1993**, *16*, 587–591. [CrossRef]

6. Kesselmeier, J.; Staudt, M. 1999. Biogenic volatile organic compounds (VOCs): An overview on emission, physiology and ecology. *J. Atmos. Chem.* **1999**, *33*, 23–88. [CrossRef]
7. Sharkey, T.D.; Wiberley, A.E.; Donohue, A.R. Isoprene emission from plants: Why and how. *Ann. Bot.* **2008**, *101*, 5–18. [CrossRef] [PubMed]
8. Brilli, F.; Barta, C.; Fortunati, A.; Lerdau, M.; Loreto, F.; Centritto, M. Response of isoprene emission and carbon metabolism to drought in white poplar (Populus alba) saplings. *New Phytol.* **2007**, *175*, 244–254. [CrossRef] [PubMed]
9. Exton, D.A.; Suggett, D.J.; McGenity, T.J.; Steinke, M. Chlorophyll-normalized isoprene production in laboratory cultures of marine microalgae and implications for global models. *Limnol. Oceanogr.* **2013**, *58*, 1301–1311. [CrossRef]
10. Dani, K.G.S.; Torzillo, G.; Michelozzi, M.; Baraldi, R.; Loreto, F. Isoprene Emission in Darkness by a Facultative Heterotrophic Green Alga. *Front. Plant Sci.* **2020**, *11*, 598786. [CrossRef] [PubMed]
11. Zhao, D.; Li, R.; Fang, G.; Tham, Y.J.; Zou, S.; Ling, Z.; Yang, Y. Isoprene emission dynamics in Chaetoceros curvisetus: Insights from transcriptome analysis under light/dark cycles. *Algal. Res.* **2024**, *82*, 103641. [CrossRef]
12. Kuzma, J.; Nemecek-Marshall, M.; Pollock, W.H.; Fall, R. Bacteria produce the volatile hydrocarbon isoprene. *Curr. Microbiol.* **1995**, *30*, 97–103. [CrossRef] [PubMed]
13. Fall, R.; Copley, S.D. Bacterial sources and sinks of isoprene, a reactive atmospheric hydrocarbon. *Environ. Microbiol.* **2000**, *2*, 123–130. [CrossRef] [PubMed]
14. Wagner, W.P.; Helmig, D.; Fall, R. Isoprene biosynthesis in Bacillus subtilis via the methylerythritol phosphate pathway. *J. Nat. Prod.* **2000**, *63*, 37–40. [CrossRef]
15. Bäck, J.; Aaltonen, H.; Hellén, H.; Kajos, M.K.; Patokoski, J.; Taipale, R.; Pumpanen, J.; Heinonsalo, J. Variable emissions of microbial volatile organic compounds (MVOCs) from root-associated fungi isolated from Scots pine. *Atmos. Environ.* **2010**, *44*, 3651–3659. [CrossRef]
16. Arnold, S.R.; Spracklen, D.V.; Williams, J.; Yassaa, N.; Sciare, J.; Bonsang, B.; Gros, V.; Peeken, I.; Lewis, A.C.; Alvain, S.; et al. Evaluation of the global oceanic isoprene source and its impacts on marine organic carbon aerosol. *Atmos. Chem. Phys.* **2009**, *9*, 1253–1262. [CrossRef]
17. Conte, L.; Szopa, S.; Aumont, O.; Gros, V.; Bopp, L. Sources and sinks of isoprene in the global open ocean: Simulated patterns and emissions to the atmosphere. *J. Geophys. Res. Oceans* **2020**, *125*, e2019JC015946. [CrossRef]
18. Luo, G.; Yu, F. A numerical evaluation of global oceanic emissions of α-pinene and isoprene. *Atmos. Chem. Phys.* **2010**, *10*, 2007–2015. [CrossRef]
19. Zhang, W.; Weber, J.; Archibald, A.T.; Abraham, N.L.; Booge, D.; Yang, M.; Gu, D. Global atmospheric composition effects from marine isoprene. *Environ. Sci. Technol.* 2025; *in press*. [CrossRef] [PubMed]
20. Zhang, W.; Gu, D. Geostationary satellite reveals increasing marine isoprene emissions in the center of the equatorial Pacific Ocean. *Npj Clim. Atmos. Sci.* **2022**, *5*, 83. [CrossRef]
21. Borbon, A.; Fontaine, H.; Veillerot, M.; Locoge, N.; Galloo, J.C.; Guillermo, R. An investigation into the traffic-related fraction of isoprene at an urban location. *Atmos. Environ.* **2001**, *35*, 3749–3760. [CrossRef]
22. Reimann, S.; Pierluigi, C.; Hofer, P. The anthropogenic fraction contribution to isoprene concentrations in a rural atmosphere. *Atmos. Environ.* **2000**, *34*, 109–115. [CrossRef]
23. Khan, M.A.H.; Schlich, B.-L.; Jenkin, M.E.; Shallcross, B.M.A.; Moseley, K.; Walker, C.; Morris, W.C.; Derwent, R.G.; Percival, C.J.; Shallcross, D.E. A two-decade anthropogenic and biogenic isoprene emissions study in a London urban background and a London urban traffic site. *Atmosphere* **2018**, *9*, 387. [CrossRef]
24. Kinoyama, M.; Nitta, H.; Watanabe, A.; Ueda, H. Acetone and isoprene concentrations in exhaled breath in healthy subjects. *J. Health Sci.* **2008**, *54*, 471–477. [CrossRef]
25. Veres, P.R.; Faber, P.; Drewnick, F.; Lelieveld, J.; Williams, J. Anthropogenic sources of VOC in a football stadium: Assessing human emissions in the atmosphere. *Atmos. Environ.* **2013**, *77*, 1052–1059. [CrossRef]
26. Kansal, A. Sources and reactivity of NMHCs and VOCs in the atmosphere: A review. *J. Hazard. Mat.* **2009**, *166*, 17–26. [CrossRef] [PubMed]
27. Sharkey, T.D.; Monson, R.K. Isoprene research—60 years later, the biology is still enigmatic. *Plant Cell Environ.* **2017**, *40*, 1671–1678. [CrossRef]
28. Steinbrecher, R.; Hauff, K.; Rabong, R.; Steinbrecher, J. Isoprenoid emission of oak species typical for the Mediterranean area: Source strength and controlling variables. *Atmos. Environ.* **1997**, *31*, 79–88. [CrossRef]
29. Jardine, K.; Monson, R.; Abrell, L.; Saleska, S.; Arneth, A.; Jardine, A.B.; Ishida, Y.; Yañez-Serrano, A.; Artaxo, P.; Karl, T.; et al. Within-plant isoprene oxidation confirmed by direct emissions of oxidation products methyl vinyl ketone and methacrolein. *Glob. Change Biol.* **2012**, *18*, 973–984. [CrossRef]
30. Vickers, C.; Possell, M.; Cojocariu, C.; Velikova, V.; Laothawornkitkul, J.; Ryan, A.; Mullineaux, P.; Hewitt, C.N. Isoprene synthesis protects transgenic tobacco plants from oxidative stress. *Plant Cell Environ.* **2009**, *32*, 520–531. [CrossRef]
31. Sanadze, G.; Kalandaze, K. Light and temperature curves of the evolution of C_5H_8. *Russ. J. Plant Physiol.* **1966**, *13*, 458–461.

32. Sharkey, T.D.; Singsaas, E.L. Why plants emit isoprene. *Nature* **1995**, *374*, 769. [CrossRef]
33. Harley, P.; Guenther, A.; Zimmerman, P. Effects of light, temperature and canopy position on net photosynthesis and isoprene emission from sweetgum (*Liquidambar styraciflua*) leaves. *Tree Physiol.* **1996**, *16*, 25–32. [CrossRef]
34. Navakoudis, E.; Lütz, C.; Langebartels, C.; Lütz-Meindl, U.; Kotzabasis, K. Ozone impact on the photosynthetic apparatus and the protective role of polyamines. *Biochim. Biophys. Acta—Gen. Subj.* **2003**, *1621*, 160–169. [CrossRef]
35. Loreto, F.; Velikova, V. Isoprene Produced by Leaves Protects the Photosynthetic Apparatus against Ozone Damage, Quenches Ozone Products, and Reduces Lipid Peroxidation of Cellular Membranes. *Plant Physiol.* **2001**, *127*, 1781–1787. [CrossRef] [PubMed]
36. Velikova, V.; Fares, S.; Loreto, F. Isoprene and nitric oxide reduce damages in leaves exposed to oxidative stress. *Plant Cell Environ.* **2008**, *31*, 1882–1894. [CrossRef]
37. Hewitt, C.N.; Kok, G.L.; Fall, R. Hydroperoxides in plants exposed to ozone mediate air pollution damage to alkene emitters. *Nature* **1990**, *344*, 56–58. [CrossRef] [PubMed]
38. Loivamaki, M.; Mumm, R.; Dicke, M.; Schnitzler, J. -P. Isoprene interferes with the attraction of bodyguards by herbaceous plants. *Proc. Natl. Acad. Sci. USA* **2008**, *105*, 17430–17435. [CrossRef]
39. Laothawornkitkul, J.; Paul, N.D.; Vickers, C.E.; Possell, M.; Taylor, J.E.; Mullineaux, P.M.; Hewitt, C.N. Isoprene emissions influence herbivore feeding decisions. *Plant Cell Environ.* **2008**, *31*, 1410–1415. [CrossRef]
40. Ganzeveld, L.; Lelieveld, J. Impact of Amazonian deforestation on atmospheric chemistry. *Geophys. Res. Lett.* **2004**, *31*, L06105. [CrossRef]
41. Leung, D.Y.C.; Wong, P.; Cheung, B.K.H.; Guenther, A. Improved land cover and emission factors for modeling biogenic volatile organic compounds emissions from Hong Kong. *Atmos. Environ.* **2010**, *44*, 1456–1468. [CrossRef]
42. Guenther, A.; Karl, T.; Harley, P.; Wiedinmyer, C.; Palmer, P.I.; Geron, C. Estimates of global terrestrial isoprene emissions using MEGAN (Model of Emissions of Gases and Aerosols from Nature). *Atmos. Chem. Phys.* **2006**, *6*, 3181–3210. [CrossRef]
43. Sindelarova, K.; Granier, C.; Bouarar, I.; Guenther, A.; Tilmes, S.; Stavrakou, T.; Müller, J.-F.; Kuhn, U.; Stefani, P.; Knorr, W. Global data set of biogenic VOC emissions calculated by the MEGAN model over the last 30 years. *Atmos. Chem. Phys.* **2014**, *14*, 9317–9341. [CrossRef]
44. Fuentes, J.D.; Wang, D.; Gu, L. Seasonal Variations in Isoprene Emissions from a Boreal Aspen Forest. *J. Appl. Meteorol.* **1999**, *38*, 855–869. [CrossRef]
45. Karl, T.; Guenther, A.; Yokelson, R.J.; Greenberg, J.; Potosnak, M.; Blake, D.R.; Artaxo, P. The tropical forest and fire emissions experiment: Emission, chemistry, and transport of biogenic volatile organic compounds in the lower atmosphere over Amazonia. *J. Geophys. Res.* **2007**, *112*, D18302. [CrossRef]
46. Pacifico, F.; Folberth, G.A.; Jones, C.D.; Harrison, S.P.; Collins, W.J. Sensitivity of biogenic isoprene emissions to past, present, and future environmental conditions and implications for atmospheric chemistry. *J. Geophys. Res.* **2012**, *117*, D22302. [CrossRef]
47. Zeng, J.; Zhang, Y.; Mu, Z.; Pang, W.; Zhang, H.; Wu, Z.; Song, W.; Wang, X. Temperature and light dependency of isoprene and monoterpene emissions from tropical and subtropical trees: Field observations in south China. *App. Geochem.* **2023**, *155*, 105727. [CrossRef]
48. Monson, R.K.; Fall, R. Isoprene emission from aspen leaves: Influence of environment and relation to photosynthesis and photorespiration. *Plant Physiol.* **1989**, *90*, 267–274. [CrossRef] [PubMed]
49. Young, P.J.; Arneth, A.; Schurgers, G.; Zeng, G.; Pyle, J.A. The CO_2 inhibition of terrestrial isoprene emission significantly affects future ozone projections. *Atmos. Chem. Phys.* **2009**, *9*, 2793–2803. [CrossRef]
50. Heald, C.L.; Wilkinson, M.J.; Monson, R.K.; Alo, C.A.; Wang, G.; Guenther, A. Response of isoprene emission to ambient CO_2 changes and implications for global budgets. *Glob. Change Biol.* **2009**, *15*, 1127–1140. [CrossRef]
51. Wilkinson, M.J.; Monson, R.K.; Trahan, N.; Lee, S.; Brown, E.; Jackson, R.B.; Polleys, H.W.; Fay, P.A.; Fall, R. Leaf isoprene emission rate as a function of atmospheric CO_2 concentration. *Glob. Change Biol.* **2009**, *15*, 1189–1200. [CrossRef]
52. Sun, Z.; Hüve, K.; Vislap, V.; Niinemets, Ü. Elevated [CO_2] magnifies isoprene emissions under heat and improves thermal resistance in hybrid aspen. *J. Exp. Bot.* **2013**, *64*, 5509–5523. [CrossRef]
53. Peeters, J.; Nguyen, T.L.; Vereecken, L. HO_x radical generation in the oxidation of isoprene. *Phys. Chem. Chem. Phys.* **2009**, *11*, 5935–5939. [CrossRef]
54. Parker, H.A.; Hasheminassab, S.; Crounse, J.D.; Roehl, C.M.; Wennberg, P.O. Impacts of traffic reductions associated with COVID-19 on southern California Air Quality. *Geophys. Res. Lett.* **2020**, *47*, e2020GL090164. [CrossRef] [PubMed]
55. van Vuuren, D.P.; Bouwman, L.F.; Smith, S.J.; Dentener, F. Global Projections for anthropogenic reactive nitrogen emissions to the atmosphere: An assessment of scenarios in the scientific literature. *Curr. Opin. Environ. Sustain.* **2011**, *3*, 359–369. [CrossRef]
56. Vinken, G.C.M.; Boersma, K.F.; Maasakkers, J.D.; Adon, M.; Martin, R.V. Worldwide biogenic soil NO_x emissions inferred from OMI NO2 observations. *Atmos. Chem. Phys.* **2014**, *14*, 10363–10381. [CrossRef]
57. Barket, D.J., Jr.; Grossenbacher, J.W.; Hurst, J.M.; Shepson, P.B.; Olszyna, K.; Thorberry, T.; Carroll, M.A.; Roberts, J.; Stroud, C.; Bottenheim, J.; et al. A study of the NO_x dependence of isoprene oxidation. *J. Geophys. Res.* **2004**, *109*, D11310. [CrossRef]

58. Denman, K.; Brasseur, G.; Chidthaisong, A.; Ciais, P.; Cox, P.; Dickinson, R.; Haugustaine, D.; Heinze, C.; Holland, E.; Jacob, D.; et al. Coupling between changes in the climate system and biogeochemistry. In *Climate Change 2007: The Physical Science Basis. Contribution of Working Group I to the Fourth Assessment Report of the Intergovernmental Panel on Climate Change*; Solomon, S., Qin, D., Manning, M., Chen, Z., Marquis, M., Averyt, K.B., Tignor, M., Miller, H.L., Eds.; Cambridge University Press: Cambridge, UK, 2007; pp. 500–587.
59. Lelieveld, J.; Butler, T.M.; Crowley, J.N.; Dillon, T.J.; Fischer, H.; Ganzeveld, L.; Harder, H.; Lawrence, M.G.; Martinez, M.; Taraborrelli, D.; et al. Atmospheric oxidation capacity sustained by a tropical forest. *Nature* **2008**, *452*, 737–740. [CrossRef] [PubMed]
60. Pugh, T.A.M.; MacKenzie, A.R.; Hewitt, C.N.; Langford, B.; Edwards, P.M.; Furneaux, K.L.; Heard, D.E.; Hopkins, J.R.; Jones, C.E.; Karunaharan, A.; et al. Simulating atmospheric composition over a South-East Asian tropical rainforest: Performance of a chemistry box model. *Atmos. Chem. Phys.* **2010**, *10*, 279–298. [CrossRef]
61. Peeters, J.; Müller, J.-F.; Stravrakou, T.; Nguyen, V.S. Hydroxyl radical recycling in isoprene oxidation driven by hydrogen bonding and hydrogen tunneling: The upgraded LIM1 mechanism. *J. Phys. Chem.* **2014**, *118*, 8625–8643. [CrossRef]
62. Hofzumahaus, A.; Rohrer, F.; Lu, K.; Bohn, B.; Brauers, T.; Chang, C.C.; Fuchs, H.; Holland, F.; Kita, K.; Kondo, Y.; et al. Amplified trace gas removal in the troposphere. *Science* **2009**, *324*, 1702–1704. [CrossRef]
63. Paulot, F.; Crounse, J.D.; Kjaergaard, H.G.; Kroll, J.H.; Seinfeld, J.H.; Wennberg, P.O. Isoprene photooxidation: New insights into the production of acids and organic nitrates. *Atmos. Chem. Phys.* **2009**, *9*, 1479–1501. [CrossRef]
64. da Silva, G.; Graham, C.; Wang, Z.-F. Unimolecular β-hydroxyperoxy radical decomposition with OH recycling in the photochemical oxidation of isoprene. *Environ. Sci. Technol.* **2010**, *44*, 250–256. [CrossRef]
65. Crounse, J.D.; Paulot, F.; Kjaergaard, H.G.; Wennberg, P.O. Peroxy radical isomerization in the oxidation of isoprene. *Phys. Chem. Chem. Phys.* **2011**, *13*, 13607–13613. [CrossRef]
66. Peeters, J.; Müller, J.-F. HO_x radical regeneration in isopreneoxidation*via*peroxy radical isomerisations. II: Experimental evidence and global impact. *Phys. Chem. Chem. Phys.* **2010**, *12*, 14227–14235. [CrossRef]
67. Nguyen, T.L.; Vereecken, L.; Peeters, J. HOx regeneration in the oxidation of isoprene III: Theoretical study of the key isomerisation of the Z-δ-hydroxy-peroxy isoprene radicals. *ChemPhysChem* **2010**, *11*, 3996–4001. [CrossRef]
68. Archibald, A.T.; Cooke, M.C.; Utembe, S.R.; Shallcross, D.E.; Derwent, R.G.; Jenkin, M.E. Impacts of mechanistic changes on HO_x formation and recycling in the oxidation of isoprene. *Atmos. Chem. Phys.* **2010**, *10*, 8097–8118. [CrossRef]
69. Hasson, A.S.; Tyndall, G.S.; Orlando, J.J.; Singh, S.; Hernandez, S.Q.; Campbell, S.; Ibarra, Y. Branching ratios for the reaction of selected carbonyl-containing peroxy radicals with hydroperoxyl radicals. *J. Phys. Chem. A* **2012**, *116*, 6264–6281. [CrossRef]
70. Teng, A.P.; Crounse, J.D.; Wennberg, P.O. Isoprene peroxy radical dynamics. *J. Am. Chem. Soc.* **2017**, *139*, 5367–5377. [CrossRef] [PubMed]
71. Xiong, F.; McAvey, K.M.; Pratt, K.A.; Groff, C.J.; Hostetler, M.A.; Lipton, M.A.; Starn, T.K.; Seeley, J.V.; Bertman, S.B.; Teng, A.P.; et al. Observation of isoprene hydroxynitrates in the southeastern United States and implications for the fate of NO_x. *Atmos. Chem. Phys.* **2015**, *15*, 11257–11272. [CrossRef]
72. Wennberg, P.O.; Bates, K.H.; Crounse, J.D.; Dodson, L.G.; McVay, R.C.; Mertens, L.A.; Nguyen, T.B.; Praske, E.; Schwantes, R.H.; Smarte, M.D.; et al. Gas-phase reactions of isoprene and its major oxidation products. *Chem. Rev.* **2018**, *118*, 3337–3390. [CrossRef]
73. Berndt, T.; Hyttinen, N.; Herrmann, H.; Hansel, A. First oxidation products from the reaction of hydroxyl radicals with isoprene for pristine environmental conditions. *Commun. Chem.* **2019**, *2*, 21. [CrossRef]
74. Müller, J.-F.; Stavrakou, T.; Peeters, J. Chemistry and deposition in the Model of Atmospheric composition at Global and Regional scales using Inversion Techniques for Trace gas Emissions (MAGRITTE v1.1)- Part 1: Chemical mechanism. *Geosci. Model Dev.* **2019**, *12*, 2307–2356. [CrossRef]
75. Novelli, A.; Vereecken, L.; Bohn, B.; Dorn, H.P.; Gkatzelis, G.I.; Hofzumahaus, A.; Holland, F.; Reimer, D.; Rohrer, F.; Rosanka, S.; et al. Importance of isomerization reactions for OH radical regeneration from the photo-oxidation of isoprene investigated in the atmospheric simulation chamber SAPHIR. *Atmos. Chem. Phys.* **2020**, *20*, 3333–3355. [CrossRef]
76. Szabó, P.; Liu, Z.; Müller, J.-F.; Harvey, J.N.; Peeters, J. Reaction pathways leading to HPALD intermediates in the OH-initiated oxidation of isoprene. *Phys. Chem. Chem. Phys.* **2024**, *26*, 26129–26137. [CrossRef] [PubMed]
77. Medeiros, D.J.; Blitz, M.A.; Seakins, P.W.; Whalley, L.K. Direct Measurements of Isoprene Autoxidation: Pinpointing Atmospheric Oxidation in Tropical Forests. *J. Am. Chem. Soc. Au* **2022**, *2*, 809–818. [CrossRef] [PubMed]
78. Jenkin, M.E.; Young, J.C.; Rickard, A.R. The MCM v3.3.1 degradation scheme for isoprene. *Atmos. Chem. Phys.* **2015**, *15*, 11433–11459. [CrossRef]
79. Jenkin, M.E.; Khan, M.A.H.; Shallcross, D.E.; Bergström, R.; Simpson, D.; Murphy, K.L.C.; Rickard, A.R. The CRI v2.2 reduced degradation scheme for isoprene. *Atmos. Environ.* **2019**, *212*, 172–182. [CrossRef]
80. Haney, J.T., Jr.; Phillips, T.; Sielken, R.L., Jr.; Valdez-Flores, C. Development of an inhalation unit risk factor for isoprene. *Regul. Toxicol. Pharmacol.* **2015**, *73*, 712–725. [CrossRef]

81. Seinfeld, J.H.; Pandis, S.N. *Atmospheric Chemistry and Physics: From Air Pollution to Climate Change*; Wiley: New York, NY, USA, 1998.
82. Bates, K.H.; Jacob, D.J. A new model mechanism for atmospheric oxidation of isoprene: Global effects on oxidants, nitrogen oxides, organic products, and secondary organic aerosol. *Atmos. Chem. Phys.* **2019**, *19*, 9613–9640. [CrossRef]
83. Chameides, W.; Lindsay, R.; Richardson, J.; Kiang, C. The Role of Biogenic Hydrocarbons in Urban Photochemical Smog: Atlanta as a Case Study. *Science* **1988**, *241*, 1473–1475. [CrossRef] [PubMed]
84. Wang, K.-Y.; Shallcross, D.E. Modelling terrestrial biogenic isoprene fluxes and its potential impact on global chemical species using a coupled LSM-CTM model. *Atmos. Environ.* **2000**, *34*, 2909–2925. [CrossRef]
85. Claeys, M.; Graham, B.; Vas, G.; Wang, W.; Vermeylen, R.; Pashynska, V.; Cafmeyer, J.; Guyon, P.; Andreae, M.O.; Artaxo, P.; et al. Formation of secondary organic aerosols through photooxidation of isoprene. *Science* **2004**, *303*, 1173–1176. [CrossRef] [PubMed]
86. Trainer, M.; Williams, E.J.; Parrish, D.D.; Buhr, M.P.; Allwine, E.J.; Westberg, H.H.; Fehsenfeld, F.C.; Liu, S.C. Models and observations of the impact of natural hydrocarbons on rural ozone. *Nature* **1987**, *329*, 705–707. [CrossRef]
87. Khan, M.A.H.; Schlich, B.-L.; Jenkin, M.E.; Cooke, M.C.; Derwent, R.G.; Neu, J.L.; Percival, C.J.; Shallcross, D.E. Changes to simulated global atmospheric composition resulting from recent revisions to isoprene oxidation chemistry. *Atmos. Environ.* **2021**, *244*, 117914. [CrossRef]
88. Fischer, E.V.; Jacob, D.J.; Yantosca, R.M.; Sulprizio, M.P.; Millet, D.B.; Mao, J.; Paulot, F.; Singh, H.B.; Roiger, A.; Ries, L.; et al. Atmospheric peroxyacetyl nitrate (PAN): A global budget and source attribution. *Atmos. Chem. Phys.* **2014**, *14*, 2679–2698. [CrossRef] [PubMed]
89. Singh, H.B. Peroxyacetyl Nitrate. In *Encyclopedia of Atmospheric Sciences*, 2nd ed.; North, G.R., Pyle, J., Zhang, F., Eds.; Academic Press: London, UK, 2015; Volume 6, pp. 251–254.
90. Kanakidou, M.; Seinfeld, J.H.; Pandis, S.N.; Barnes, I.; Dentener, F.J.; Facchini, M.C.; Van Dingenen, R.; Ervens, B.; Nenes, A.; Nielsen, C.J.; et al. Organic aerosol and global climate modelling: A review. *Atmos. Chem. Phys.* **2005**, *5*, 1053–1123. [CrossRef]
91. Scott, C.E.; Rap, A.; Spracklen, D.V.; Forster, P.M.; Carslaw, K.S.; Mann, G.W.; Pringle, K.J.; Kivekäs, N.; Kulmala, M.; Lihavainen, H.; et al. The direct and indirect radiative effects of biogenic secondary organic aerosol. *Atmos. Chem. Phys.* **2014**, *14*, 447–470. [CrossRef]
92. Pandis, S.N.; Paulson, S.E.; Seinfeld, J.H.; Flagan, R.C. Aerosol formation in the photooxidation of isoprene and β-pinene. *Atmos. Environ.* **1991**, *25*, 997–1008. [CrossRef]
93. Carlton, A.G.; Wiedinmyer, C.; Kroll, J.H. A review of secondary organic aerosol (SOA) formation from isoprene. *Atmos. Chem. Phys.* **2009**, *9*, 4987–5005. [CrossRef]
94. Surratt, J.D.; Chan, A.W.H.; Eddingsaas, N.C.; Chan, M.; Loza, C.L.; Kwan, A.J.; Hersey, S.P.; Flagan, R.C.; Wennberg, P.O.; Seinfeld, J.H. Reactive intermediates revealed in secondary organic aerosol formation from isoprene. *Proc. Natl. Acad. Sci. USA* **2010**, *107*, 6640–6645. [CrossRef] [PubMed]
95. Rap, A.; Scott, C.E.; Spracklen, D.V.; Bellouin, N.; Forster, P.M.; Carslaw, K.S.; Schmidt, A.; Mann, G. Natural aerosol direct and indirect radiation effects. *Geophys. Res. Lett.* **2013**, *40*, 3297–3301. [CrossRef]
96. Curtius, J.; Heinritzi, M.; Beck, L.J.; Pöhlker, M.L.; Tripathi, N.; Krumm, B.E.; Holzbeck, P.; Nussbaumer, C.M.; Pardo, L.H.; Klimach, T.; et al. Isoprene nitrates drive new particle formation in Amazon's upper troposphere. *Nature* **2024**, *636*, 124–130. [CrossRef]
97. Shen, J.; Russell, D.M.; DeVivo, J.; Kunkler, F.; Baalbaki, R.; Mentler, B.; Scholz, W.; Yu, W.; Caudillo-Plath, L.; Sommer, E.; et al. New particle formation from isoprene under upper-tropospheric conditions. *Nature* **2024**, *636*, 115–123. [CrossRef] [PubMed]
98. Pye, H.O.T.; Ward-Caviness, C.K.; Murphy, B.N.; Appel, K.W.; Seltzer, K.M. Secondary organic aerosol association with cardiorespiratory disease mortality in the United States. *Nat. Commun.* **2021**, *12*, 7215. [CrossRef] [PubMed]
99. Stavrakou, T.; Peeters, J.; Müller, J.-F. Improved global modelling of HO_x recycling in isoprene oxidation: Evaluation against the GABRIEL and INTEX-A aircraft campaign measurements. *Atmos. Chem. Phys.* **2010**, *10*, 9863–9878. [CrossRef]
100. Archibald, A.T.; Levine, J.G.; Abraham, N.L.; Cooke, M.C.; Edwards, P.M.; Heard, D.E.; Jenkin, M.E.; Karunaharan, A.; Pike, R.C.; Monks, P.S.; et al. Impacts of HO_x regeneration and recycling in the oxidation of isoprene: Consequences for the composition of past, present and future atmospheres. *Geophys. Res. Lett.* **2011**, *38*, L05804. [CrossRef]
101. Utembe, S.R.; Watson, L.A.; Shallcross, D.E.; Jenkin, M.E. A Common Representative Intermediates (CRI) mechanism for VOC degradation. Part 3: Development of a secondary organic aerosol module. *Atmos. Environ.* **2009**, *43*, 1982–1990. [CrossRef]
102. Watson, L.A.; Shallcross, D.E.; Utembe, S.R.; Jenkin, M.E. A Common Representative Intermediate (CRI) mechanism for VOC degradation. Part 2: Gas phase mechanism reduction. *Atmos. Environ.* **2008**, *42*, 7196–7204. [CrossRef]
103. Jenkin, M.E.; Watson, L.A.; Utembe, S.R.; Shallcross, D.E. A Common Representative Intermediate (CRI) mechanism for VOC degradation. Part-1: Gas phase mechanism development. *Atmos. Environ.* **2008**, *42*, 7185–7195. [CrossRef]
104. Weber, J.; Archer-Nicholls, S.; Griffiths, P.; Berndt, T.; Jenkin, M.; Gordon, H.; Knote, C.; Archibald, A.T. CRI-HOM: A novel chemical mechanism for simulating highly oxygenated organic molecules (HOMs) in global chemistry-aerosol-climate models. *Atmos. Chem. Phys.* **2020**, *20*, 10889–10910. [CrossRef]

105. Atkinson, R.; Arey, J. Gas-phase tropospheric chemistry of biogenic volatile organic compounds. *Atmos. Environ.* **2003**, *37*, 197–219. [CrossRef]
106. Yáñez-Serrano, A.M.; Bourtsoukidis, E.; Alves, E.G.; Bauwens, M.; Stavrakou, T.; Llusià, J.; Filella, I.; Guenther, A.; Williams, J.; Artaxo, P.; et al. Amazonian biogenic volatile organic compounds under global change. *Glob. Change Biol.* **2020**, *26*, 4722–4751. [CrossRef] [PubMed]
107. Bottenheim, J.W.; Shepherd, M.F. C2–C6 hydrocarbon measurements at four rural locations across Canada. *Atmos. Environ.* **1995**, *29*, 647–664. [CrossRef]
108. Jobson, B.T.; Wu, Z.; Niki, H.; Barrie, L.A. Seasonal trends of isoprene, C2-C5 alkanes, and acetylene at a remote boreal site in Canada. *J. Geophys. Res.* **1994**, *99*, 1589–1599. [CrossRef]
109. Montzka, S.A.; Trainer, M.; Goldan, P.D.; Kuster, W.C.; Fehsenfeld, F.C. Isoprene and its oxidation products, methyl vinyl ketone and methacrolein, in the rural troposphere. *J. Geophys. Res.* **1993**, *98*, 1101–1111. [CrossRef]
110. Apel, E.C.; Riemer, D.D.; Hills, A.; Baugh, W.; Orlando, J.; Faloona, I.; Tan, D.; Brune, W.; Lamb, B.; Westberg, H.; et al. Measurement and interpretation of isoprene fluxes and isoprene, methacrolein, and methyl vinyl ketone mixing ratios at the PROPHET site during the 1998 Intensive. *J. Geophys. Res.-Atmos.* **2002**, *107*, 4034. [CrossRef]
111. Rhew, R.C.; Deventer, M.J.; Turnipseed, A.A.; Warneke, C.; Ortega, J.; Shen, S.; Martinez, L.; Koss, A.; Lerner, B.M.; Gilman, J.B.; et al. Ethene, propene, butene and isoprene emissions from a ponderosa pine forest measured by relaxed eddy accumulation. *Atmos. Chem. Phys.* **2017**, *17*, 13417–13438. [CrossRef]
112. Link, M.; Zhou, Y.; Taubman, B.; Sherman, J.; Morrow, H.; Krintz, I.; Robertson, L.; Cook, R.; Stocks, J.; West, M.; et al. A characterization of volatile organic compounds and secondary organic aerosol at a mountain site in the Southeastern United States. *J. Atmos. Chem.* **2015**, *72*, 81–104. [CrossRef]
113. Dreyfus, G.B.; Schade, G.W.; Goldstein, A.H. Observational constraints on the contribution of isoprene oxidation to ozone production on the western slope of the Sierra Nevada, California. *J. Geophys. Res.-Atmos.* **2002**, *107*, 4365. [CrossRef]
114. Rasmussen, R.A.; Khalil, M.A. Isoprene over the Amazon basin. *J. Geophys. Res.* **1988**, *93*, 1417–1421. [CrossRef]
115. Greenberg, J.P.; Zimmerman, P.R. Nonmethane hydrocarbons in remote tropical, continental and marine atmospheres. *J. Geophys. Res.* **1984**, *89*, 4767–4778. [CrossRef]
116. Zimmerman, P.R.; Greenberg, J.P.; Westberg, C.E. Measurements of atmospheric hydrocarbons and biogenic emission fluxes in the Amazon boundary layer. *J. Geophys. Res.* **1988**, *93*, 1407–1416. [CrossRef]
117. Alves, E.G.; Jardine, K.; Tota, J.; Jardine, A.; Yãnez-Serrano, A.M.; Karl, T.; Tavares, J.; Nelson, B.; Gu, D.; Stavrakou, T.; et al. Seasonality of isoprenoid emissions from a primary rainforest in central Amazonia. *Atmos. Chem. Phys.* **2016**, *16*, 3903–3925. [CrossRef]
118. Kesselmeier, J.; Kuhn, U.; Wolf, A.; Andreae, M.; Ciccioli, P.; Brancaleoni, E.; Frattoni, M.; Guenther, A.; Greenberg, J.; De Castro Vasconcellos, P.; et al. Atmospheric volatile organic compounds (VOC) at a remote tropical forest site in central Amazonia. *Atmos. Environ.* **2000**, *34*, 4063–4072. [CrossRef]
119. Yáñez-Serrano, A.M.; Nölscher, A.C.; Williams, J.; Wolff, S.; Alves, E.; Martins, G.A.; Bourtsoukidis, E.; Brito, J.; Jardine, K.; Artaxo, P.; et al. Diel and seasonal changes of biogenic volatile organic compounds within and above an Amazonian rainforest. *Atmos. Chem. Phys.* **2015**, *15*, 3359–3378. [CrossRef]
120. Kuhn, U.; Andreae, M.O.; Ammann, C.; Araújo, A.C.; Brancaleoni, E.; Ciccioli, P.; Dindorf, T.; Frattoni, M.; Gatti, L.V.; Ganzeveld, L.; et al. Isoprene and monoterpene fluxes from Central Amazonian rainforest inferred from tower-based and airborne measurements, and implications on the atmospheric chemistry and the local carbon budget. *Atmos. Chem. Phys.* **2007**, *7*, 2855–2879. [CrossRef]
121. Langford, B.; House, E.; Valach, A.; Hewitt, C.N.; Artaxo, P.; Barkley, M.P.; Brito, J.; Carnell, E.; Davison, B.; MacKenzie, A.R.; et al. Seasonality of isoprene emissions and oxidation products above the remote Amazon. *Environ. Sci.-Atmos.* **2022**, *2*, 230–240. [CrossRef]
122. Helmig, D.; Balsley, B.; Davis, K.; Kuck, L.R.; Jensen, M.; Bognar, J.; Smith, T., Jr.; Arrieta, R.V.; Rodriguez, R.; Birks, J.W. Vertical profiling and determination of landscape fluxes of biogenic nonmethane hydrocarbons within the planetary boundary layer in the Peruvian Amazon. *J. Geophys. Res. Atmos.* **1998**, *103*, 25519–25532. [CrossRef]
123. Donoso, L.; Romero, R.; Rondon, A.; Fernandez, E.; Oyola, P.; Sanhueza, E. Natural and anthropogenic C2 to C6 hydrocarbons in the central-eastern Venezuelan atmosphere during the rainy season. *J. Atmos. Chem.* **1996**, *25*, 201–214. [CrossRef]
124. Holzinger, R.; Sanhueza, E.; von Kuhlmann, R.; Kleiss, B.; Donoso, L.; Crutzen, P.J. Diurnal cycles and seasonal variation of isoprene and its oxidation products in the tropical savanna atmosphere. *Glob. Biogeochem. Cycles* **2002**, *16*, 1074. [CrossRef]
125. Warneke, C.; Holzinger, R.; Hansel, A.; Jordan, A.; Lindinger, W.; Pöschl, U.; Williams, J.; Hoor, P.; Fischer, H.; Crutzen, P.J.; et al. Isoprene and its oxidation products methyl vinyl ketone, methacrolein, and isoprene related peroxides measured online over the tropical rain forest of Surinam in March 1998. *J. Atmos. Chem.* **2001**, *38*, 167–185. [CrossRef]

126. Emmerson, K.M.; Galbally, I.E.; Guenther, A.B.; Paton-Walsh, C.; Guerette, E.-A.; Cope, M.E.; Keywood, M.D.; Lawson, S.J.; Molloy, S.B.; Dunne, E.; et al. Current estimates of biogenic emissions from eucalypts uncertain for southeast Australia. *Atmos. Chem. Phys.* **2016**, *16*, 6997–7011. [CrossRef]
127. Jones, C.E.; Hopkins, J.R.; Lewis, A.C. In situ measurements of isoprene and monoterpenes within a south-east Asian tropical rainforest. *Atmos. Chem. Phys.* **2011**, *11*, 6971–6984. [CrossRef]
128. Langford, B.; Misztal, P.K.; Nemitz, E.; Davison, B.; Helfter, C.; Pugh, T.A.M.; MacKenzie, A.R.; Lim, S.F.; Hewitt, C.N. Fluxes and concentrations of volatile organic compounds from a South-East Asian tropical rainforest. *Atmos. Chem. Phys.* **2010**, *10*, 8391–8412. [CrossRef]
129. Liu, T.; Yan, D.; Chen, G.; Lin, Z.; Zhu, C.; Chen, J. Distribution characteristics and photochemical effects of isoprene in a coastal city of southeast China. *Sci. Total Environ.* **2024**, *956*, 177392. [CrossRef] [PubMed]
130. Gu, C.; Wang, S.; Zhu, J.; Wu, S.; Duan, Y.; Gao, S.; Zhou, B. Investigation on the urban ambient isoprene and its oxidation processes. *Atmos. Environ.* **2022**, *270*, 118870. [CrossRef]
131. Gong, D.; Wang, H.; Zhang, S.; Wang, Y.; Liu, S.C.; Guo, H.; Shao, M.; He, C.; Chen, D.; He, L.; et al. Low-level summertime isoprene observed at a forested mountaintop site in southern China: Implications for strong regional atmospheric oxidative capacity. *Atmos. Chem. Phys.* **2018**, *18*, 14417–14432. [CrossRef]
132. Wang, C.; Huang, X.-F.; Han, Y.; Zhu, B.; He, L. -Y. Sources and Potential Photochemical Roles of Formaldehyde in an Urban Atmosphere in South China. *J. Geophys. Res. Atmos.* **2017**, *122*, 11934–11947. [CrossRef]
133. Wang, J.L.; Chew, C.; Chang, C.Y.; Liao, W.C.; Lung, S.C.C.; Chen, W.N.; Lee, P.J.; Lin, P.H.; Chang, C.C. Biogenic isoprene in subtropical urban settings and implications for air quality. *Atmos. Environ.* **2013**, *79*, 369–379. [CrossRef]
134. Wu, F.; Yu, Y.; Sun, J.; Zhang, J.; Wang, J.; Tang, G.; Wang, Y. Characteristics, source apportionment and reactivity of ambient volatile organic compounds at Dinghu Mountain in Guangdong Province, China. *Sci. Total Environ.* **2016**, *548–549*, 347–359. [CrossRef]
135. Chen, H.W.; Ho, K.F.; Lee, S.C.; Nichol, J.E. Biogenic volatile organic compounds (BVOC) in ambient air over Hong Kong: Analytical methodology and field measurement. *Int. J. Environ. Anal. Chem.* **2010**, *90*, 988–998. [CrossRef]
136. Tang, J.H.; Chan, L.Y.; Chang, C.C.; Liu, S.; Li, Y.S. Characteristics and sources of non-methane hydrocarbons in background atmospheres of eastern, southwestern, and southern China. *J. Geophys. Res.-Atmos.* **2009**, *114*, D03304. [CrossRef]
137. Wang, T.; Guo, H.; Blake, D.R.; Kwok, Y.H.; Simpson, I.J.; Li, Y.S. Measurements of trace gases in the inflow of South China Sea background air and outflow of regional pollution at Tai O, Southern China. *J. Atmos. Chem.* **2005**, *52*, 295–317. [CrossRef]
138. Zhu, Y.; Yang, L.; Kawamura, K.; Chen, J.; Ono, K.; Wang, X.; Xue, L.; Wang, W. Contributions and source identification of biogenic and anthropogenic hydrocarbons to secondary organic aerosols at Mt. Tai in 2014. *Environ. Pollut.* **2017**, *220*, 863–872. [CrossRef] [PubMed]
139. Xue, L.K.; Wang, T.; Guo, H.; Blake, D.R.; Tang, J.; Zhang, X.C.; Saunders, S.M.; Wang, W.X. Sources and photochemistry of volatile organic compounds in the remote atmosphere of western China: Results from the Mt. Waliguan Observatory. *Atmos. Chem. Phys.* **2013**, *13*, 8551–8567. [CrossRef]
140. Kalogridis, C.; Gros, V.; Sarda-Esteve, R.; Langford, B.; Loubet, B.; Bonsang, B.; Bonnaire, N.; Nemitz, E.; Genard, A.-C.; Boissard, C.; et al. Concentrations and fluxes of isoprene and oxygenated VOCs at a French Mediterranean oak forest. *Atmos. Chem. Phys.* **2014**, *14*, 10085–10102. [CrossRef]
141. Acton, W.J.F.; Schallhart, S.; Langford, B.; Valach, A.; Rantala, P.; Fares, S.; Carriero, G.; Tillmann, R.; Tomlinson, S.J.; Dragosits, U.; et al. Canopy-scale flux measurements and bottom-up emission estimates of volatile organic compounds from a mixed oak and hornbeam forest in northern Italy. *Atmos. Chem. Phys.* **2016**, *16*, 7149–7170. [CrossRef]
142. Seco, R.; Peñuelas, J.; Filella, I.; Llusià, J.; Molowny-Horas, R.; Schallhart, S.; Metzger, A.; Müller, M.; Hansel, A. Contrasting winter and summer VOC mixing ratios at a forest site in the Western Mediterranean Basin: The effect of local biogenic emissions. *Atmos. Chem. Phys.* **2011**, *11*, 13161–13179. [CrossRef]
143. Ferracci, V.; Weber, J.; Bolas, C.G.; Robinson, A.D.; Tummon, F.; Rodríguez-Ros, P.; Cortés-Greus, P.; Baccarini, A.; Jones, R.L.; Galí, M.; et al. Atmospheric isoprene measurements reveal larger-than-expected Southern Ocean emissions. *Nat. Commun.* **2024**, *15*, 2571. [CrossRef]
144. Millet, D.B.; Jacob, D.J.; Boersma, K.F.; Fu, T.-M.; Kurosu, T.P.; Chance, K.; Heald, C.L.; Guenther, A. Spatial distribution of isoprene emissions from North America derived from formaldehyde column measurements by the OMI satellite sensor. *J. Geophys. Res.* **2008**, *113*, D02307. [CrossRef]
145. Stavrakou, T.; Müller, J.-F.; De Smedt, I.; Van Roozendael, M.; van der Werf, G.R.; Giglio, L.; Guenther, A. Global emissions of non-methane hydrocarbons deduced from SCIAMACHY formaldehyde columns through 2003–2006. *Atmos. Chem. Phys.* **2009**, *9*, 3663–3679. [CrossRef]
146. Barkley, M.P.; Smedt, I.D.; Roozendael, M.V.; Kurosu, T.P.; Chance, K.; Arneth, A.; Hagberg, D.; Guenther, A.; Paulot, F.; Marais, E.; et al. Top-down isoprene emissions over tropical South America inferred from SCIAMACHY and OMI formaldehyde columns. *J. Geophys. Res. Atmos.* **2013**, *118*, 6849–6868. [CrossRef]

147. Marais, E.A.; Jacob, D.J.; Guenther, A.; Chance, K.; Kurosu, T.P.; Murphy, J.G.; Reeves, C.E.; Pye, H.O.T. Improved model of isoprene emissions in Africa using Ozone Monitoring Instrument (OMI) satellite observations of formaldehyde: Implications for oxidants and particulate matter. *Atmos. Chem. Phys.* **2014**, *14*, 7693–7703. [CrossRef]
148. Bauwens, M.; Stavrakou, T.; Müller, J.-F.; De Smedt, I.; Roozendael, M.V.; van der Werf, G.R.; Wiedinmyer, C.; Kaiser, J.W.; Sindelarova, K.; Guenther, A. Nine years of global hydrocarbon emissions based on source inversion of OMI formaldehyde observations. *Atmos. Chem. Phys.* **2016**, *16*, 10133–10158. [CrossRef]
149. Kaiser, J.; Jacob, D.J.; Zhu, L.; Travis, K.R.; Fisher, J.A.; Abad, G.G.; Zhang, L.; Zhang, X.; Fried, A.; Crounse, J.D.; et al. High-resolution inversion of OMI formaldehyde columns to quantify isoprene emission on ecosystem-relevant scales: Application to the southeast US. *Atmos. Chem. Phys.* **2018**, *18*, 5483–5497. [CrossRef]
150. Palmer, P.I.; Jacob, D.J.; Fiore, A.M.; Martin, R.V.; Chance, K.; Kurosu, T.P. Mapping isoprene emissions over North America using formaldehyde column observations from space. *J. Geophys. Res. Atmos.* **2003**, *108*, 4180. [CrossRef]
151. Müller, J.-F.; Stavrakou, T.; Oomen, G.-M.; Opacka, B.; De Smedt, I.; Guenther, A.; Vigouroux, C.; Langerock, B.; Aquino, C.A.B.; Grutter, M.; et al. Bias correction of OMI HCHO columns based on FTIR and aircraft measurements and impact on top-down emission estimates. *Atmos. Chem. Phys.* **2024**, *24*, 2207–2237. [CrossRef]
152. Opacka, B.; Müller, J.-F.; Stavrakou, T.; Miralles, D.G.; Koppa, A.; Pagán, B.R.; Potosnak, M.J.; Seco, R.; De Smedt, I.; Guenther, A.B. Impact of Drought on Isoprene Fluxes Using Field Data, Satellite-Based GLEAM Soil Moisture and HCHO Observations from OMI. *Remote Sens.* **2022**, *14*, 2021. [CrossRef]
153. Zheng, Y.; Unger, N.; Tadiæ, J.M.; Seco, R.; Guenther, A.B.; Barkley, M.P.; Potosnak, M.J.; Murray, L.T.; Michalak, A.M.; Qiu, X.; et al. Drought impacts on photosynthesis, isoprene emission and atmospheric formaldehyde in a mid-latitude forest. *Atmos. Environ.* **2017**, *167*, 190–201. [CrossRef]
154. Wolfe, G.M.; Kaiser, J.; Hanisco, T.F.; Keutsch, F.N.; de Gouw, J.A.; Gilman, J.B.; Graus, M.; Hatch, C.D.; Holloway, J.; Horowitz, L.W.; et al. Formaldehyde production from isoprene oxidation across NO_x regimes. *Atmos. Chem. Phys.* **2016**, *16*, 2597–2610. [CrossRef] [PubMed]
155. Marais, E.A.; Jacob, D.J.; Kurosu, T.P.; Chance, K.; Murphy, J.G.; Reeves, C.; Mills, G.; Casadio, S.; Millet, D.B.; Barkley, M.P.; et al. Isoprene emissions in Africa inferred from OMI observations of formaldehyde columns. *Atmos. Chem. Phys.* **2012**, *12*, 6219–6235. [CrossRef] [PubMed]
156. Fu, D.; Millet, D.B.; Wells, K.C.; Payne, V.H.; Yu, S.; Guenther, A.; Eldering, A. Direct retrieval of isoprene from satellite-based infrared measurements. *Nat Commun* **2019**, *10*, 3811. [CrossRef]
157. Wells, K.C.; Millet, D.B.; Payne, V.H.; Vigouroux, C.; Aquino, C.A.B.; De Mazière, M.; de Gouw, J.A.; Graus, M.; Kurosu, T.; Warneke, C.; et al. Next-generation isoprene measurements from space: Detecting daily variability at high resolution. *J. Geophys. Res. Atmos.* **2022**, *127*, e2021JD036181. [CrossRef]
158. Wells, K.C.; Millet, D.B.; Payne, V.H.; Deventer, M.J.; Bates, K.H.; de Gouw, J.A.; Graus, M.; Warneke, C.; Wisthaler, A.; Fuentes, J.D. Satellite isoprene retrievals constrain emissions and atmospheric oxidation. *Nature* **2020**, *585*, 225–233. [CrossRef]
159. Ashworth, K.; Wild, O.; Hewitt, C.N. Sensitivity of isoprene emissions estimated using MEGAN to the time resolution of input climate data. *Atmos. Chem. Phys.* **2010**, *10*, 1193–1201. [CrossRef]
160. Pugh, T.A.M.; Ashworth, K.; Wild, O.; Hewitt, C.N. Effects of the spatial resolution of climate data on estimates of biogenic isoprene emissions. *Atmos. Environ.* **2013**, *70*, 1–6. [CrossRef]
161. Situ, S.; Wang, X.; Guenther, A.; Zhang, Y.; Wang, X.; Huang, M.; Fan, Q.; Xiong, Z. Uncertainties of isoprene emissions in the MEGAN model estimated for a coniferous and broad-leaved mixed forest in Southern China. *Atmos. Environ.* **2014**, *98*, 105–110. [CrossRef]
162. Filella, I.; Zhang, C.; Seco, R.; Potosnak, M.; Guenther, A.; Karl, T.; Gamon, J.; Pallardy, S.; Gu, L.; Kim, S.; et al. A MODIS photochemical reflectance index (PRI) as an estimator of isoprene emissions in a temperate deciduous forest. *Remote Sens.* **2018**, *10*, 557. [CrossRef]
163. Sarkar, C.; Guenther, A.B.; Park, J.-H.; Seco, R.; Alves, E.; Batalha, S.; Santana, R.; Kim, S.; Smith, J.; Tóta, J.; et al. PTR-TOF-MS eddy covariance measurements of isoprene and monoterpene fluxes from an eastern Amazonian rainforest. *Atmos. Chem. Phys.* **2020**, *20*, 7179–7191. [CrossRef]
164. DiMaria, C.A.; Jones, D.B.A.; Worden, H.; Bloom, A.A.; Bowman, K.; Starvrakou, T.; Miyazaki, K.; Worden, J.; Guenther, A.; Sarkar, C.; et al. Optimizing the isoprene emission model MEGAN with satellite and ground-based observational constraints. *J Geophys. Res. Atmos.* **2023**, *128*, e2022JD037822. [CrossRef]
165. Houghton, R.A.; Shroder, J.F.; Sivanpillai, R. *Biological and Environmental Hazards, Risks, and Disasters*; Academic Press: Boston, MA, USA, 2016; pp. 313–315.
166. Scott, C.E.; Monks, S.A.; Spracklen, D.V.; Arnold, S.R.; Forster, P.M.; Rap, A.; Äijälä, M.; Artaxo, P.; Carslaw, K.S.; Chipperfield, M.P.; et al. Impact on short-lived climate forcers increases projected warming due to deforestation. *Nat. Commun.* **2018**, *9*, 157. [CrossRef] [PubMed]

167. Novick, K.A.; Katul, G.G. The Duality of Reforestation Impacts on Surface and Air Temperature. *J. Geophys. Res. Biogeosci.* **2020**, *125*, e2019JG005543. [CrossRef]
168. Avissar, R.; Werth, D. Global Hydroclimatological Teleconnections Resulting from Tropical Deforestation. *J. Hydrometeorol.* **2005**, *6*, 134–145. [CrossRef]
169. Foley, J.A.; Costa, M.H.; Delire, C.; Ramankutty, N.; Snyder, P. Green surprise? How terrestrial ecosystems could affect earth's climate. *Front. Ecol. Environ.* **2003**, *1*, 38–44. [CrossRef]
170. Raupach, M.R. Vegetation-atmosphere interaction in homogeneous and heterogeneous terrain: Some implications of mixed-layer dynamics. *Vegetatio* **1991**, *91*, 105–120. [CrossRef]
171. Li, Y.; Zhao, M.; Motesharrei, S.; Mu, Q.; Kalnay, E.; Li, S. Local cooling and warming effects of forests based on satellite observations. *Nat. Commun.* **2015**, *6*, 6603. [CrossRef] [PubMed]
172. Davin, E.; de Noblet-Ducoudré, N. Climatic Impact of Global-Scale Deforestation: Radiative versus Nonradiative Processes. *J. Clim.* **2010**, *23*, 97–112. [CrossRef]
173. Lee, X.; Goulden, M.L.; Hollinger, D.Y.; Barr, A.; Black, T.A.; Bohrer, G.; Bracho, R.; Drake, B.; Goldstein, A.; Gu, L.; et al. Observed Increase in Local Cooling Effect of Deforestation at Higher Latitudes. *Nature* **2011**, *479*, 384–387. [CrossRef]
174. Bruijnzeel, L.A.; Bonell, M.; Costa, M.H. *Forests, Water and People in the Humid Tropics: Past, Present and Future Hydrological Research for Integrated Land and Water Management*; Cambridge University Press: Cambridge, UK, 2005; pp. 590–597.
175. Zhang, Q.; Barnes, M.; Benson, M.; Burakowski, E.; Oishi, A.C.; Ouimette, A.; Sanders-DeMott, R.; Stoy, P.C.; Wenzel, M.; Xiong, L.; et al. Reforestation and surface cooling in temperate zones: Mechanisms and implications. *Glob. Change Biol.* **2020**, *26*, 3384–3401. [CrossRef] [PubMed]
176. Bastin, J.-F.; Finegold, Y.; Garcia, C.; Mollicone, D.; Rezende, M.; Routh, D.; Zohner, C.M.; Crowther, T.W. The global tree restoration potential. *Science* **2019**, *365*, 76–79. [CrossRef] [PubMed]
177. Arino, O.; Ramos Perez, J.J.; Kalogirou, V.; Bontemps, S.; Defourny, P.; Van Bogaert, E. Global Land Cover Map for 2009 (GlobCover 2009), PANGAEA, European Space Agency & Université catholique de Louvain (UCL). *PANGAEA* **2012**. [CrossRef]
178. Veldman, J.W.; Aleman, J.C.; Alvarado, S.T.; Anderson, T.M.; Archibald, S.; Bond, W.J.; Boutton, T.W.; Buchmann, N.; Buisson, E.; Canadell, J.G.; et al. Comment on "The global tree restoration potential". *Science* **2019**, *366*, 7976. [CrossRef] [PubMed]
179. Friedlingstein, P.; Allen, M.; Canadell, J.G.; Peters, G.P.; Seneviratne, S.I. Comment on "The global tree restoration potential". *Science* **2019**, *366*, 8060. [CrossRef] [PubMed]
180. Welz, O.; Savee, J.D.; Osborn, D.L.; Vasu, S.S.; Percival, C.J.; Shallcross, D.E.; Taatjes, C.A. Direct kinetic measurements of Criegee intermediate (CH_2OO) formed by reaction of CH_2I with O_2. *Science* **2012**, *335*, 204–207. [CrossRef] [PubMed]
181. McGillen, M.R.; Curchod, B.F.E.; Chhantyal-Pun, R.; Beames, J.M.; Watson, N.; Khan, M.A.H.; McMahon, L.; Shallcross, D.E.; Orr-Ewing, A.J. Criegee intermediate-alcohol reactions, a potent source of functionalized hydroperoxides in the atmosphere. *ACS Earth Space Chem.* **2017**, *1*, 664–672. [CrossRef]
182. Chhantyal-Pun, R.; Khan, M.A.H.; Taatjes, C.A.; Percival, C.J.; Orr-Ewing, A.J.; Shallcross, D.E. Criegee intermediates: Production, detection and reactivity. *Int. Rev. Phys. Chem.* **2020**, *39*, 385–424. [CrossRef]